Tectonophysics 690 (2016) 97–116

Contents lists available at ScienceDirect

Tectonophysics

journal homepage: www.elsevier.com/locate/tecto

Reservoir leakage along concentric faults in the Southern North Sea: Implications for the deployment of CCS and EOR techniques

Nicholas I.P. Ward *, Tiago M. Alves, Tom G. Blenkinsop

3D Seismic Lab, School of Earth and Ocean Sciences, Cardiff University, Main Building-Park Place, Cardiff CF10 3AT, United Kingdom

ARTICLE INFO

Article history:
Received 29 October 2015
Received in revised form 22 July 2016
Accepted 25 July 2016
Available online 27 July 2016

Keywords:
North Sea
Concentric faults
Salt-withdrawal
Carbon capture and storage
Fluid flow
Slip tendency

ABSTRACT

High-quality 3D seismic and borehole data in the Broad Fourteens Basin, Southern North Sea, is used to investigate newly recognised concentric faults formed in salt-withdrawal basins flanking reactivated salt structures. Throw-depth and throw-distance plots were used to understand the growth histories of individual faults. As a result, three families of concentric faults are identified: a) intra-seal faults within a salt-withdrawal basin, b) faults connecting the seal and the reservoir on the crest of an inverted anticline, c) raft-bounding faults propagating into reservoir units. They have moved obliquely and show normal throws, even though they formed during a period of regional compression. Faults in the salt-withdrawal basin and on the inverted anticline are highly segmented, increasing the chances of compartmentalisation or localised fluid flow through fault linkages. Slip tendency analysis was carried out on the distinct fault families to compare the likelihood of slip along a fault at different pore fluid pressures and within different lithologies. Our results show that sections of the faults are optimally oriented with regards to maximum horizontal stresses (σ_{Hmax}), increasing the slip tendency. The identified faults cut through a variety of lithologies, allowing different values of pore fluid pressures to build up before faults reactivate. Within the Vlieland Sandstones, pore fluid pressures of 30 MPa are not sufficient to reactivate pre-existing faults, whereas in the deeper Posidonia Shales faults might reactivate at pore fluid pressures of 25 MPa. Fluid flow features preferentially occur near fault segments close to failure. Heterogeneity in slip tendency along concentric faults, and high degrees of fault segmentation, present serious hazards when injecting CO_2 into the subsurface. This study stresses the importance of high-quality 3D seismic data and the need to evaluate individual fault systems when investigating potential reservoirs for carbon capture and storage and enhanced oil recovery.

1. Introduction

Concentric faults are curved structural features formed in response to the evacuation of subsurface sediment and ensuing basin subsidence (Alsop, 1996; Bertoni and Cartwright, 2005; Ge and Jackson, 1998; Maione and Pickford, 2001; Price and Cosgrove, 1990; Stewart, 1999, 2006; Underhill, 2009). Concentric faults have been documented above collapsed salt diapirs (Bertoni and Cartwright, 2005; Cartwright et al., 2001; Stewart, 2006), but few studies have discussed them in salt-withdrawal basins (Maione and Pickford, 2001; Underhill, 2004). In this work, high quality 3D seismic data has unveiled some of these concentric faults within, and proximal to, a salt-withdrawal basin generated in the Broad Fourteens Basin, Southern North Sea (Fig. 1a–c). They have a net normal separation, have reactivated obliquely and formed during a period of compression, demonstrating a compound history (Maione and Pickford, 2001; Nalpas et al., 1995; Oudmayer and De Jager, 1993). Their occurrence may present an important caveat for the implementation of carbon capture and storage (CCS), and enhanced oil recovery (EOR) techniques, in strata flanking salt structures in the North Sea and in equivalent salt-rich basins (Cawley et al., 2015).

In the Southern North Sea, the dominant control on concentric fault distribution is the movement of Zechstein salt, which is present throughout most of the offshore region of the Netherlands (Alves and Elliott, 2014; Verweij and Simmelink, 2002). The majority of hydrocarbon discoveries in the Dutch sector of the North Sea are within conventional anticlinal traps and fault-dip closures (Herber and De Jager, 2010; Van Hulten, 2010b). However, the gradual decline in production and increasing costs of maintaining current infrastructure has led to a greater emphasis on understanding oil and gas plays in more complex structures, with the ultimate aim of deploying CCS and EOR techniques in otherwise mature fields (Lokhorst and Wildenborg, 2005; Van Hulten, 2010a) and in Jurassic source intervals (Weijermars, 2013). The implementation of these techniques, however, may be impeded by faults and other structural complexities, which can act both as conduits and barriers to fluid flow (Bentham et al., 2013; Cartwright et al., 2007). For example, active faults that cross-cut seal units may allow fluid to escape to the surface. In parallel, tectonically 'locked' faults may be reactivated if fluid pressure reduces the effective stress so that faults become critically stressed (Wiprut and Zoback, 2000, 2002). Conversely, faults that are barriers to

* Corresponding author.
E-mail address: wardni@cardiff.ac.uk (N.I.P. Ward).

http://dx.doi.org/10.1016/j.tecto.2016.07.027

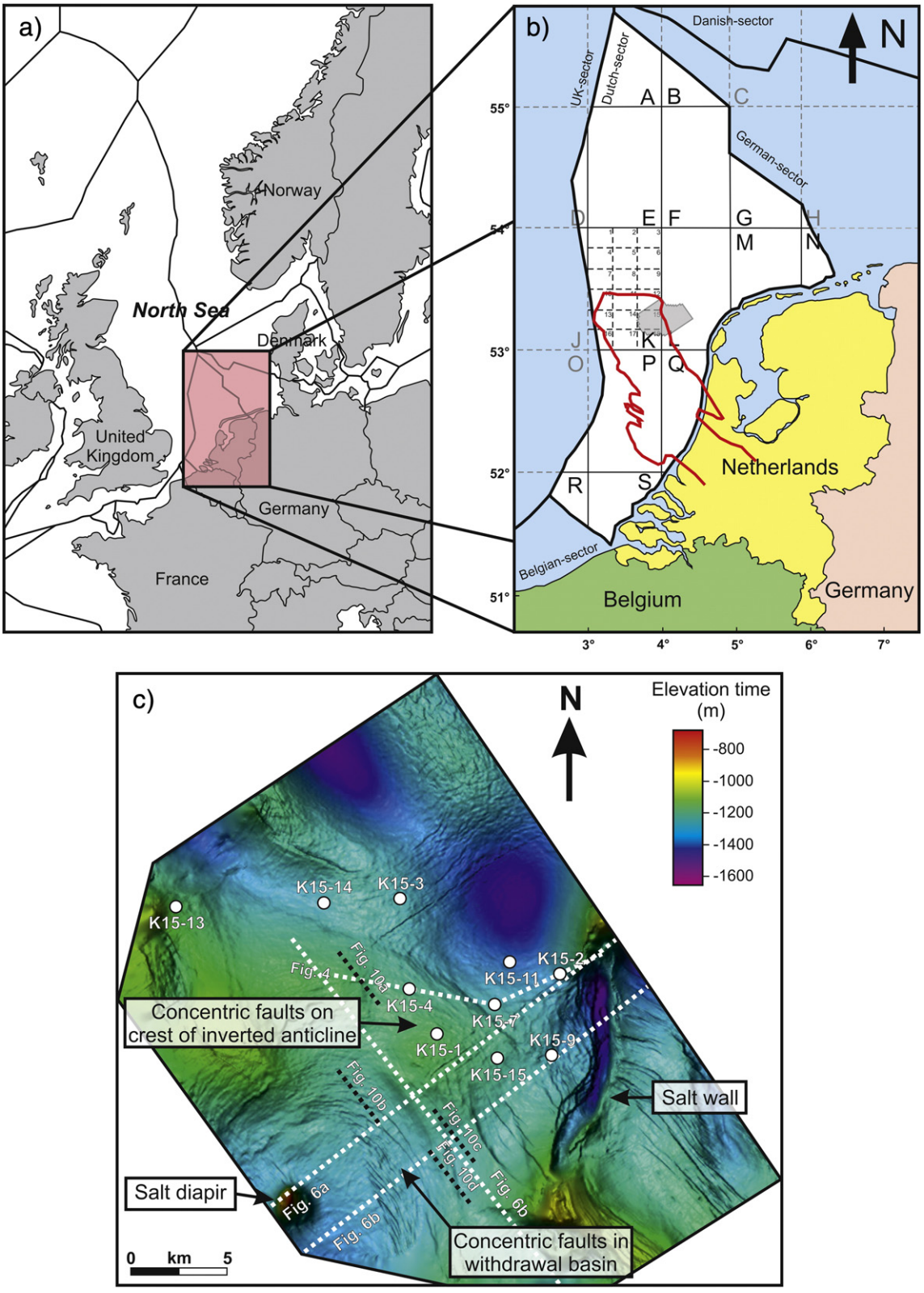

Fig. 1. a) Map of Western Europe, political and continental shelf boundaries. b) Enlarged location map of the Dutch sector of the Southern North Sea showing its relative position in Western Europe. The Broad Fourteens Basin is highlighted by the red contour line, whereas the 3D seismic survey used in this paper is shaded in the grey box. c) Interpreted Horizon H6 (Base Tertiary) displaying key features of this study, the wells interpreted in the study area, and seismic lines shown in this paper.

fluid flow could potentially compartmentalise reservoir units, resulting in an increase in costs as more wells are needed to retrieve hydrocarbons (Hardman and Booth, 1991).

This study aims to understand the evolution of concentric faults and the effects they have on seal integrity in a hydrocarbon producing region where CCS and EOR techniques are being implemented (Fig. 1a–

b). Feasibility studies into CCS are being deployed in the Broad Fourteens Basin as of 2015, including in Block K15 where the study area is located (Bentham et al., 2013; Neele et al., 2012). In this paper, fault growth and propagation histories are assessed using throw-depth (*t-z*) and throw-distance (*t-x*) plots. Displacement data provide information on nucleation, segmentation, linkage and reactivation along a fault (Baudon and Cartwright, 2008; Omosanya and Alves, 2014). The likelihood for faults to slip and act as fluid-flow pathways is quantitatively analysed in this work by calculating slip tendency for interpreted fault families (Morris et al., 1996). The modelling of increasing pore fluid pressures along concentric faults demonstrates the effects fluid injection (CCS) might have on the seal integrity. In summary, the following research questions are addressed in this paper:

a) What is the propagation history of the concentric faults and how did they form?
b) How does the timing of hydrocarbon maturation and migration relate to concentric faults?
c) What are the implications of finding concentric faults for the implementation of CCS and EOR techniques?

2. Data and methods

The 3D seismic volume interpreted in this work covers ~842 km^2 of the Broad Fourteens Basin (BFB), offshore Netherlands (Fig. 1a–b). The seismic volume has an inline spacing of 25 m, and was processed to a 25 m × 25 m bin. Vertical resolution reaches ~10 m based on seismic-borehole ties (Figs. 2, 3 and 4). Fifteen well logs were tied to the seismic data to correlate the horizons and constrain the stratigraphy across the study area (Figs. 1c, 3 and 4). Correlation panels between different wells show thickness variations and the absence of strata on the footwall of the larger faults (Fig. 3).

Schlumberger's Petrel® was used to interpret six key seismic horizons (Fig. 5). Seismic horizons were mapped across the study area so that root-mean-square (RMS) amplitude and variance maps could be computed to provide clear images of faults and gas pipes (Alves and Elliott, 2014; Brown et al., 2004). Mapped horizons highlight the changes in fault architecture and fluid pipe morphology through the Mesozoic stratigraphic sequences (Fig. 5). Once identified, fault surfaces were mapped manually every five composite lines (~125 m), perpendicular to strike. These data were exported to Midland Valley Move™ so that slip tendency and fluid flow analyses could be undertaken. Slip tendency enables the thorough assessment of stress states and its effects on the potential for fault activity. Slip is largely dependent on the frictional characteristics of rocks and the ratio of shear stress (τ) to normal stress (σ_n) (Alves and Elliott, 2014; McFarland et al., 2012; Morris et al., 1996). Therefore, slip tendency (T_s) is calculated as:

$$T_s = \tau/\sigma_{n\ \mathrm{eff}} = \tau/(\sigma_n - P_f). \quad (1)$$

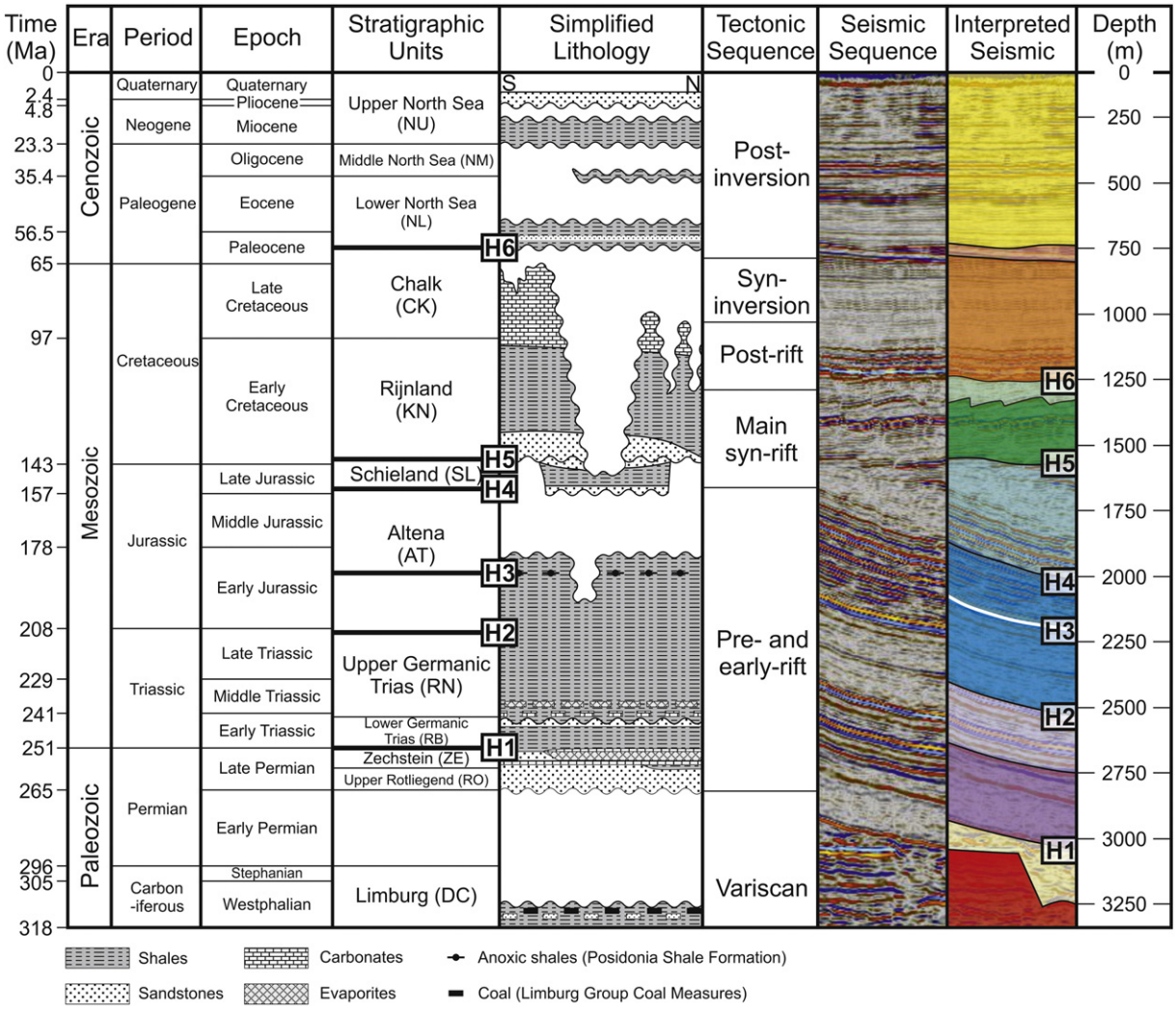

Fig. 2. Stratigraphic units, main lithologies and tectonic sequences in the Broad Fourteens Basin. Seismic data and interpretations are included as well as key horizons. Lithologies, ages and depths are based on interpreted borehole data. Modified from Alves and Elliott (2014), and Verweij and Simmelink (2002).

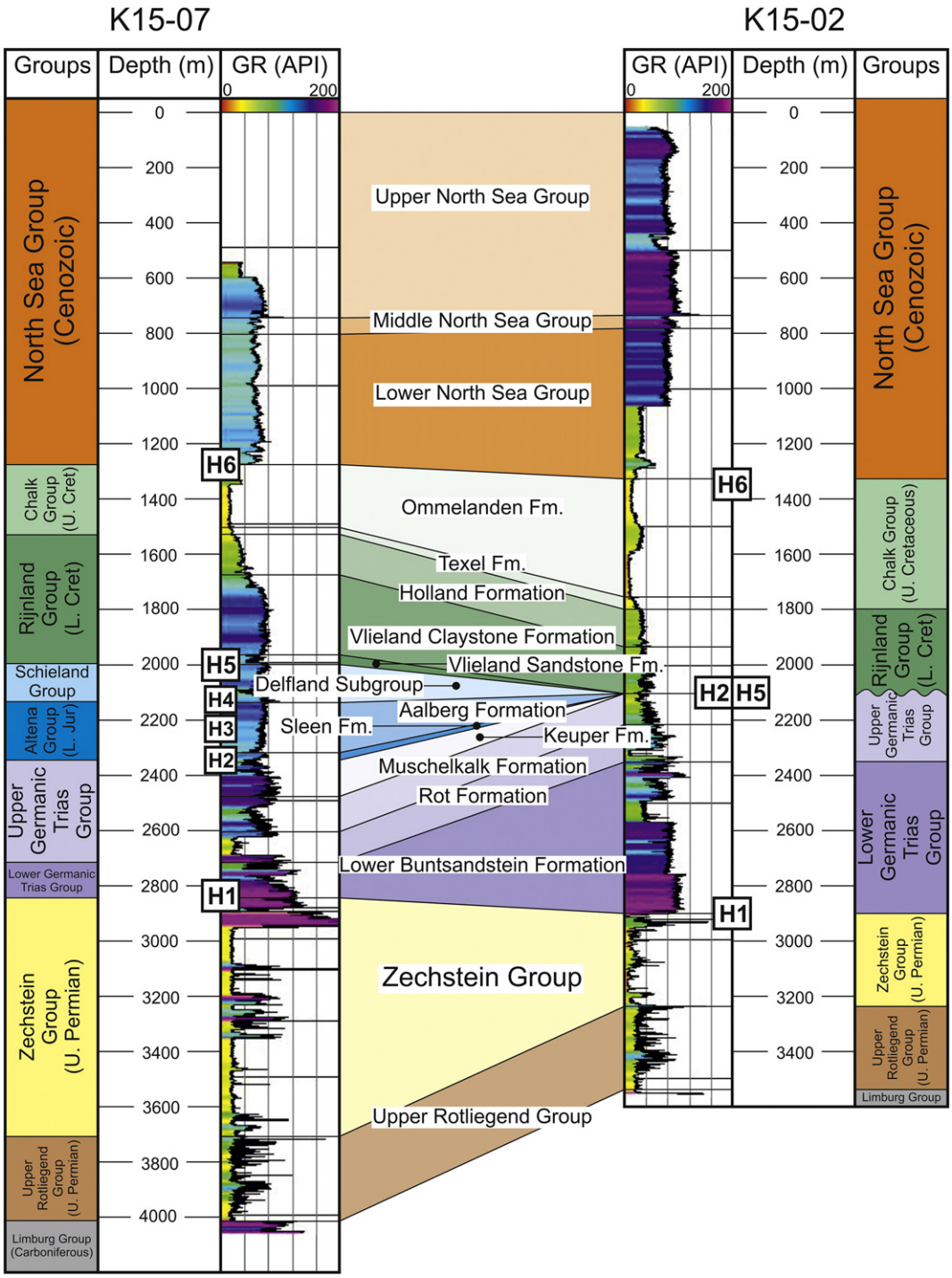

Fig. 3. Correlation panel between wells K15-02 and K15-07. See Fig. 1c for location. This figure highlights the thickness variations observed across the study area. K15-07 is a well drilled through the inversion crest, whereas well K15-02 is located close to a salt diapir in the east of the 3D seismic volume. Gamma Ray (GR) logs are measured in American Petroleum Institute (API) units.

Present-day differential stresses found in the Broad Fourteens Basin were estimated for use in the slip tendency model. Principal stress orientations were based on measurements proximal to the Broad Fourteens Basin using the World Stress Map (Heidbach et al., 2008). Stress magnitudes were calculated using the style of deformation in the basin and the proposed depth of injection for CCS.

At present the Broad Fourteens is experiencing oblique-dextral compression derived from tectonic activity in the Alps, which accommodate convergence between the African and Eurasian Plates (Frikken, 1999; Heidbach et al., 2008; Verweij and Simmelink, 2002). As a result of this setting, $\sigma_{Hmax} = \sigma_1$, $\sigma_v = \sigma_2$, and $\sigma_{hmin} = \sigma_3$ (Heidbach et al., 2008). Using an average clastic rock density of 2.3 g cm^{-3} and a hydrostatic pressure gradient increase of ~10 MPa km^{-1}, the vertical principal stress increases at a rate of 23 MPa km^{-1} (Zoback, 2010).

An average depth of 1500 m was estimated for the interpreted fault families based on well data, with the resulting vertical principal stress approaching 35 MPa. According to Andersonian Fault theory (Anderson, 1951), compressive fault regimes (strike-slip or reverse faults) have similar values of σ_3 and σ_v; i.e. the ratio of σ_3/σ_v is close to 1. Grollimund et al. (2001) postulate a σ_3/σ_v ratio between 0.9 and

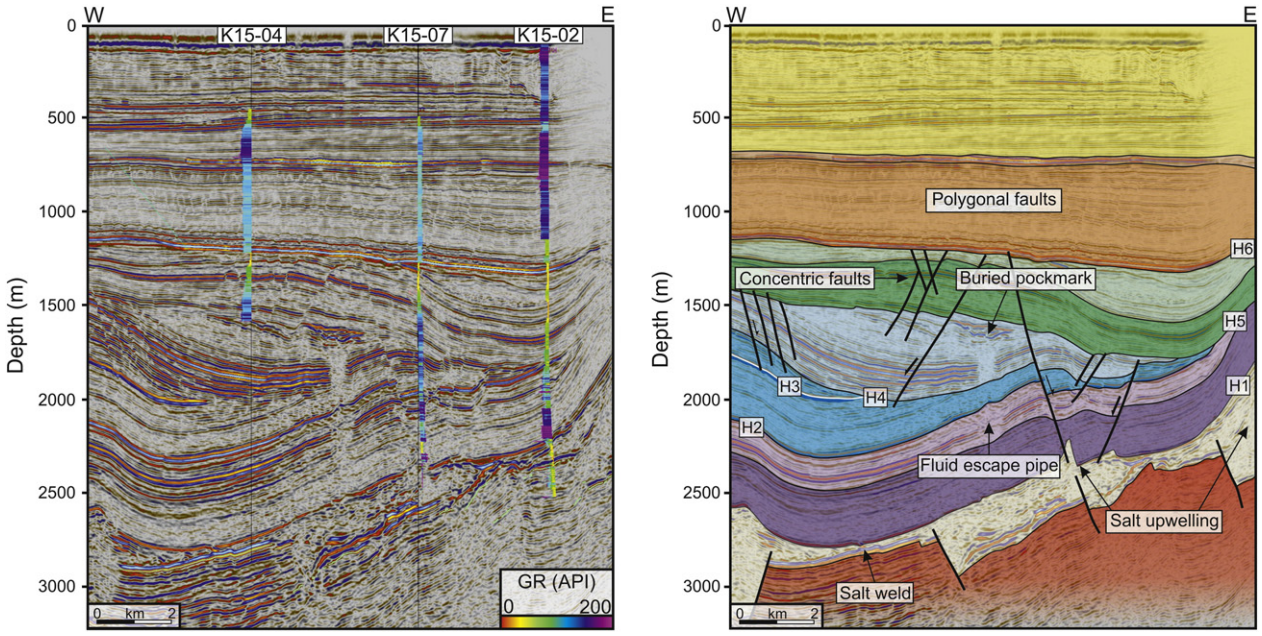

Fig. 4. Wells K15-04, K15-07 and K15-02 are tied to seismic data to help identify different lithologies and seismic-stratigraphic units. Both interpreted and uninterpreted seismic sections are shown. The section used is highlighted in Fig. 1c Colours in Fig. 3 correspond to those used in this figure for distinct stratigraphic units. The wells are gamma-ray logs (GR) and measure in American Petroleum Institute (API) units.

1 for the southern Norwegian North Sea, commenting on similar stress conditions throughout NW Europe. As faults are currently undergoing oblique-reverse movements in the study area, the ratio of 0.9 was used in the stress analyses. Therefore: $\sigma_{hmin} = 0.9\,\sigma_v \sim 31.5$ MPa. Sensitivity tests show that slight variations of σ_{hmin} (± 0.1) does not dramatically change the results of the paper. The stress difference ratio (Φ) can be used to calculate the maximum horizontal stress (Alves and Elliott, 2014; Morris et al., 1996):

$$\Phi = (\sigma_2 - \sigma_3)/(\sigma_1 - \sigma_3). \quad (2)$$

An average stress difference ratio value of 0.25 was calculated for present day conditions, making $\sigma_{Hmax} = 45.5$ MPa (Hillis and Nelson, 2005; Newnes, 2014; van Gent et al., 2009). The stress difference ratio value varies has a range of ± 0.13, although an average for the wide data range seemed appropriate, even though σ_{Hmax} would change by a maximum of ± 15 MPa (Hillis and Nelson, 2005; Newnes, 2014; van Gent et al., 2009).

The effective normal stress used for slip tendency analyses takes into account pore fluid pressure (P_f). As the fluid pressure increases, the effective stress decreases, making a fault more likely to slip (Handin et al., 1963). At the depth in which concentric faults are located, pore fluids appear to hydrostatic, i.e., they have no overpressure (Verweij and Simmelink, 2002). Injecting CO_2 into reservoirs at this depth will therefore increase the pore fluid pressure.

Throw-depth (*t-z*) and throw-distance (*t-x*) analyses were performed to understand fault propagation histories (Baudon and Cartwright, 2008; Jackson and Rotevatn, 2013; Mansfield and Cartwright, 1996; Omosanya and Alves, 2014). Throw values were measured along the same composite lines used to map the faults. Using *t-z* plots, the age and depth of fault reactivation can be estimated, as well as the horizon reactivation took place on. The mode of vertical propagation of fault could be distinguished using *t-z* plots (Baudon and Cartwright, 2008). The resulting *t-x* plots show the history of lateral propagation and give evidence of any fault segment linkage (Cartwright et al., 1995).

3. Geological setting

3.1. Evolution of the Broad Fourteens Basin

The Broad Fourteens Basin, part of the larger South Permian Basin, records a complex history of rifting, halokinesis and inversion (Duin et al., 2006; Nalpas et al., 1995; Van Wijhe, 1987; Verweij and Simmelink, 2002; Ziegler, 1990). It was formed during the Mesozoic in response to E-W opening of the Atlantic Ocean (Verweij and Simmelink, 2002). Therefore, the evolution of the basin can be divided into three intervals with distinct deformation histories: a) Carboniferous-Permian; b) Triassic-Jurassic; c) Late Cretaceous-Cenozoic.

3.1.1. Carboniferous-Permian pre-rift evolution

Towards the end of the Carboniferous, the Variscan Foreland basin developed in the Southern North Sea. Thick lacustrine and deltaic intervals with interbedded coal seams were deposited as part of the Limburg Group. Included in this unit are the Westphalian Coal Measures, a major source of gas in the Southern North Sea (Gerling et al., 1999; Van Wijhe, 1987). Oblique-slip normal faulting predominated after the Variscan Orogeny, with the largest faults cutting through the Variscan fold belt and propagating along older NW-SE trending basement faults. The present-day structural grain of the Southern North Sea follows horst and graben structures formed by these faults (Duin et al., 2006; Oudmayer and De Jager, 1993; Van Wijhe, 1987; Ziegler, 1990) (Figs. 1 and 5).

Sedimentation in the Permian was interrupted by thermal upwelling from dolerite intrusions through oblique-slip dextral normal faults. This hiatus is expressed in the form of a Saalian unconformity separating Lower from Upper Rotliegend strata (Van Wees et al., 2000). Subsidence resumed in the Late Permian, and the South Permian Basin became separated from the North Permian Basin by the Mid North Sea High (Duin et al., 2006). Upper Rotliegend terrestrial sandstones of the Slochteren Formation were deposited above the Saalian unconformity and became the major reservoir for the Permian gas plays (Verweij and Simmelink, 2002).

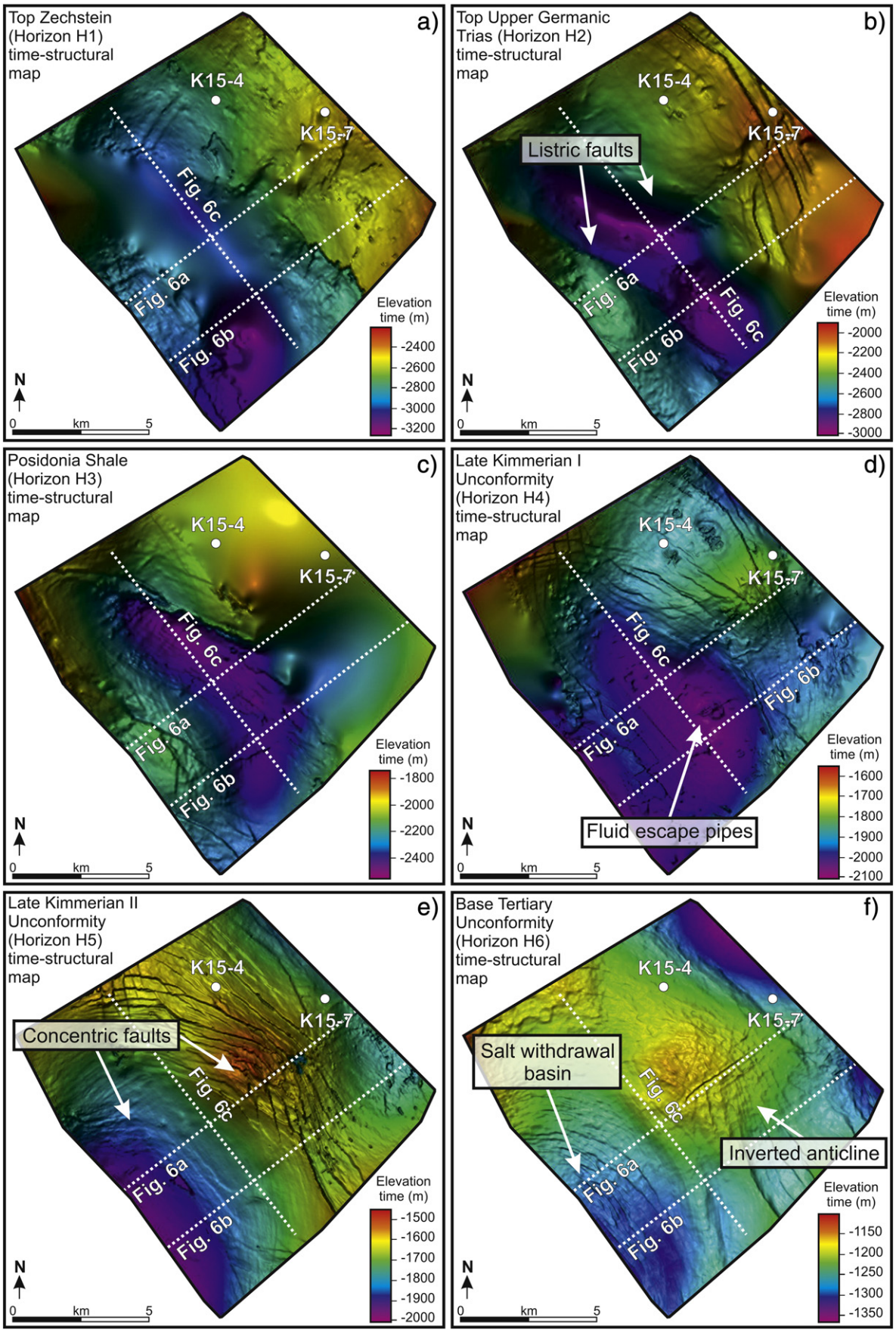

Fig. 5. Structural maps of all the seismic horizons mapped in the study area. Locations of wells tied to seismic data in Fig. 3 and the seismic profile of Fig. 4 are highlighted in this figure. All important features are identified on selected horizons.

The Zechstein Sea subsequently flooded the study area in the Latest Permian. Carbonate-evaporite cycles in Zechstein evaporites reflect fluctuations in sea level (Fig. 3), but thick deposits of Zechstein evaporites in the North of the Broad Fourteens Basin became an effective seal rock for Permian gas plays (Coward, 1995).

3.1.2. Triassic-Jurassic syn-rift evolution

Rifting intensified during the Triassic, allowing for differential subsidence in the Southern North Sea (Alves and Elliott, 2014; Duin et al., 2006). In the rapidly subsiding Broad Fourteens Basin, aeolian sands and lacustrine claystones from the Lower and Upper Germanic Trias Group were deposited (Fig. 2). The Lower Buntsandstein is a prolific reservoir for Permian gas, particularly where Zechstein salt has been withdrawn and welds have formed between Triassic rocks and the Rotliegend Group (Van Hulten, 2010b). Towards the end of the Triassic salt tectonics and reactive diapirism became concentrated along extensional boundary faults (Stewart and Coward, 1995; Ziegler, 1992). Rift-raft tectonics led to the further deepening of the Broad Fourteens Basin and open marine conditions (Alves and Elliott, 2014; Penge et al., 1993). As a result, the deepwater Altena Shales were deposited in the Broad Fourteens Basin, with the more bituminous Posidonia Shale Formation comprising the source interval for Jurassic oil plays, despite a significant isolation of the Southern North Sea in confined sub-basins (Duin et al., 2006; Nalpas et al., 1995).

Deposition of the Altena Shales stopped in the Middle Jurassic during the Mid-Kimmerian upwarping event. In areas of greatest uplift, up to 1500 m of Jurassic rocks were eroded (Heim et al., 2013). Despite this localised uplift event, sharp pulses of NE-SW rifting continued to rotate the Broad Fourteens Basin to its present day orientation. Increased erosion of Triassic, Zechstein and Rotliegend rocks on structural highs generated thick successions of the Delfland Subgroup and Vlieland Sandstone — both reservoirs for oil sourced from Posidonia Shale (Duin et al., 2006; Van Wijhe, 1987; Verweij and Simmelink, 2002).

3.1.3. Late Cretaceous-Cenozoic basin inversion and its impact on maturation curves

A major episode of sea-level rise, accompanied by post-rift subsidence, led to the accumulation of thick layers of chalk both in individual basins and on the marginal highs (Van Wijhe, 1987; Verweij and Simmelink, 2002). In the Turonian, N-S Alpine compression interrupted subsidence and Subhercynean inversion reactivated Variscan faults with a reverse-dextral motion (De Lugt et al., 2003; Nalpas et al., 1995). In such a setting, the localisation of a salt (Zechstein) décollement layer to the North of the Broad Fourteens Basin accounts for the lack of connectivity between sub-salt and supra-salt faults (Van Wijhe, 1987). Maximum erosion (~3000 m) took place in the centre of the inverted basin, close to the axis of inversion (De Lugt et al., 2003; Nalpas et al., 1995).

Three additional inversion events took place in the Broad Fourteens Basin, separated by periods of subsidence. The Laramide inversion in the Cenozoic reactivated Subhercynean faults, creating a prominent Cretaceous-Tertiary unconformity (De Lugt et al., 2003; Oudmayer and De Jager, 1993). Major basin inversion events are recorded in the Cenozoic, the largest of which coincided with the Pyrenean Orogeny (Oligocene) and created an unconformity at the base of the Miocene (Oudmayer and De Jager, 1993; Verweij and Simmelink, 2002). It separated the Lower North Sea Group from the Middle North Sea Group (Wong et al., 2001). The boundary between the Middle and Upper North Sea Groups is based on a break of sedimentation resulting from regional uplift and global low in sea level, associated with the Alpine Orogeny (Savian unconformity, Middle Miocene) (Oudmayer and De Jager, 1993; Wong et al., 2001).

3.2. Concentric faults on diapir crests vs. concentric faults in salt-withdrawal basins

Concentric faults surrounding salt structures initiate during both the rise and fall of diapirs. The expansion and upward movement of an intruding diapir can cause concentric faults to form around the margin of the diapir head. Steep, normal faults caused by the shearing of the salt body accommodate the strain, dipping away from the diapir (Stewart, 2006). Rejuvenation of active diapirism by lateral compression may cause concentric faults to form above the salt diapir. Steep or reverse concentric faults grow in overlying strata and root to the top of the diapir, dipping towards its core (Stewart, 2006). Similar concentric faults form during salt dissolution and collapse (or shrinking) of a salt body. The accommodation space created by removal of salt and shrinking of the diapir creates normal faults that dip towards the centre of the diapir (Bertoni and Cartwright, 2005).

The style of concentric faults adjacent to and above salt diapirs differs from concentric faults formed within salt-withdrawal basins, as discussed in this paper. Evacuation of salt and subsidence of the overlying strata forms secondary rim synclines marginal to the salt diapir itself. Faults dip towards the basin centre rather than towards the salt body itself, dipping either away from or towards the salt diapir (Stewart, 2006).

4. Seismic stratigraphy

The main seismic units interpreted in this study are bounded by regional unconformities. Each unit consists of a series of mapped horizons (Figs. 4 and 5). In this section, nineteen (19) wells were tied to the interpreted seismic volume. Exploration wells K15-02, K15-04, and K15-07 were used to describe the lithologies crossed by the wells and illustrate stratal thickness variations across the interpreted seismic volume (Fig. 3).

Well K15-02 was drilled close to a salt wall, on the footwall of a listric, south-dipping fault (Figs. 1c and 4). Well K15-07 was drilled on a Late Cretaceous inverted anticline. This well crossed a relatively thin Upper Jurassic interval and an intrusion of salt at a depth of 2205 m. Well K15-04 reached its maximum depth at the base of the Rijnland Group, but a deviation well K15-04-S2 continued through to the Permian Rotliegendes Group. It was drilled SW of a large listric fault, recording the thickest succession of Schieland Group (~640 m) (Figs. 1c and 4). No wells were drilled in either the crest of the inverted anticline or the SW salt-withdrawal basin, so seismic horizons in this zone were tied to the wells closer to this region.

4.1. Rotliegend Group sandstones (Autunian to Tatarian)

The Rotliegend Group sandstones are the deepest resolvable unit on 3D seismic data (Fig. 6a–c). A bright reflection along the upper boundary separates the Upper Rotliegend from the Zechstein Group. Similar gamma-ray curves in wells K15-07 and K15-02 reflect an abundance of sand in both locations. Maxima in gamma-ray values on these logs indicate localised accumulations of gas (Fig. 3). The drilled Rotliegend sandstones consist largely of terrestrial course grained deposits (e.g. Slochteren Formation) and finer grained desert lake deposits (e.g. Silverpit Formation) (Verweij and Simmelink, 2002).

Parallel reflections are truncated by large E-W trending Variscan faults (Fig. 6a–c). These faults can reach displacement values of ~300 m. The base of the unit is hard to identify because the overlying salt dims the internal reflections of Rotliegend strata. There is little variation in thickness across the basin, irrespective of large fault displacements (Fig. 6a–c).

4.2. Zechstein Group (Late Permian)

A high-amplitude seismic reflection separates the Zechstein from the Rotliegend Groups (Figs. 4 and 5a). The upper boundary of the

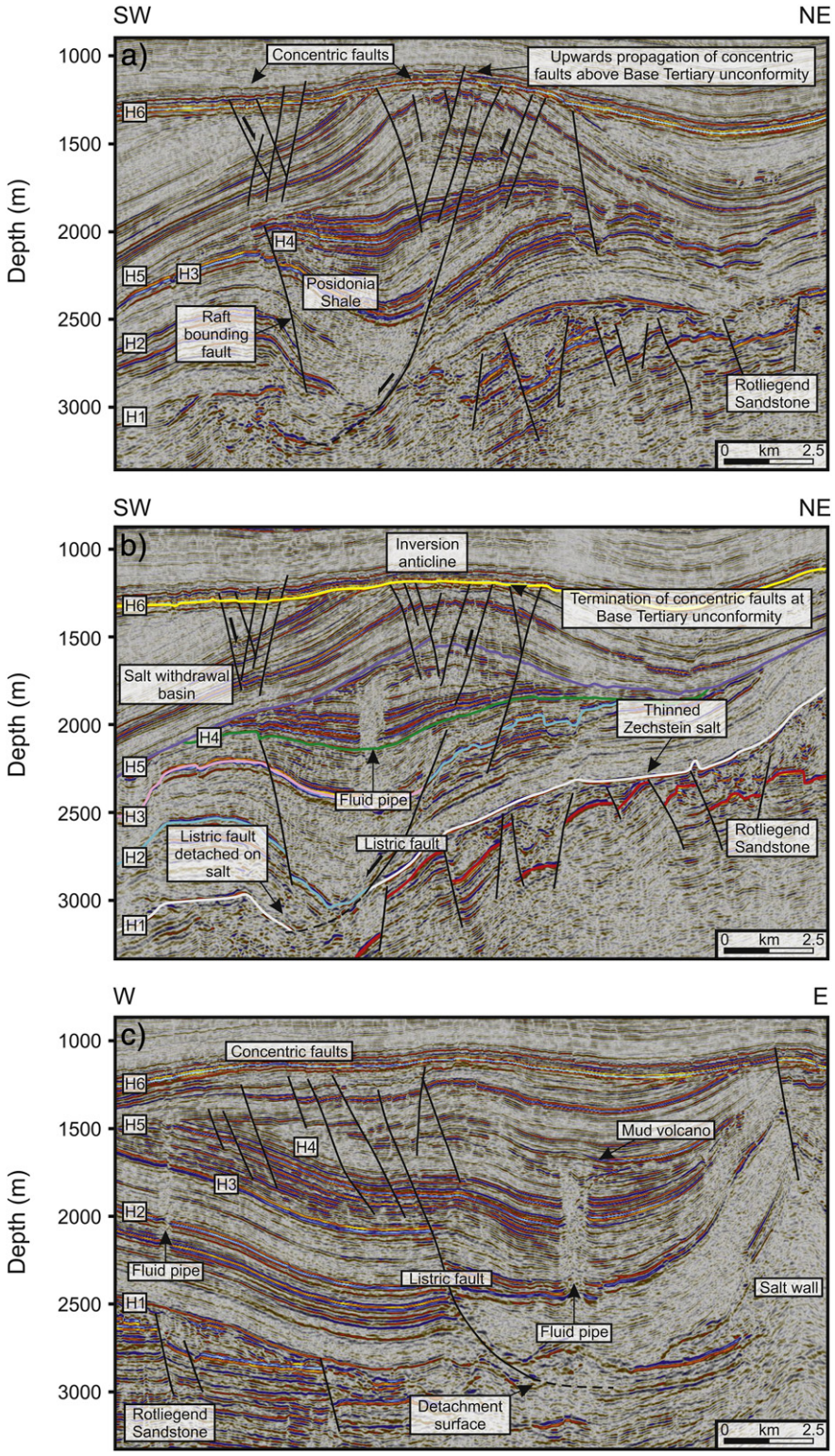

Fig. 6. Interpreted seismic profiles highlighting the styles of faulting and fluid flow in the study area. a) SW-NE section identifying fault types. In this section, the concentric faults on the crest of the inverted anticline propagate above the Base Tertiary unconformity. b) SW-NE section showing fluid escape pipes, concentric faults truncated by H6, and thinning of Zechstein salt. c) W-E section showing evidence of fluid escape and an interpreted mud volcano at the upper terminus of a fluid pipe. The raft-bounding listric fault detaches in Zechstein salt.

Zechstein Group is a continuous mid-high amplitude reflection (Horizon H1) that is disrupted where salt has penetrated through younger Triassic rocks, forming salt diapirs (Figs. 3 and 4). Low amplitude, chaotic internal reflections onlap the faulted internal reflections typical of the Rotliegend Group (Fig. 4). Where salt has completely evacuated, the bottom reflection connects to the top reflection H1 (Fig. 6b).

Low gamma-ray values are typical of thick salt layers (Passey et al., 1990). Fig. 3 shows the presence of thick layers of salt separated by cyclic carbonate intervals (Coward, 1995). This figure also shows marked thickness variations across a small distance. At the top of the Zechstein Salt there is a unit of rocks with high gamma-ray values that can be traced between wells (Fig. 3).

4.3. Upper and Lower Germanic Trias Groups (Latest Permian to Norian)

The Trias Group comprises Triassic siliciclastic rocks (Verweij and Simmelink, 2002). The bright reflection at the base (Horizon H1) indicates a change from high-velocity Zechstein evaporites to relatively low-velocity aeolian sandstones and lacustrine claystones of the Lower Germanic Trias Group (~500 m thick) (Figs. 3 and 4). The Lower Buntsandstein Formation has a similar gamma-ray character in wells K15-07 and K15-02. However, well K15-07 is situated on the crest of an inverted anticline and has a condensed section showing a similar decreasing gamma-ray trend above the Zechstein Salt (Fig. 3).

High gamma-ray values at the base of the Lower Germanic Trias Group indicate a higher content in organic matter, which continues at least 50 m into the Zechstein Group (Figs. 3 and 4). The transition between Zechstein Evaporites and Lower Buntsandstein Formation is the Zechstein Upper Claystone Formation (Van Adrichem Boogaert and Kouwe, 1994–1997). The overlying Upper Germanic Trias Group comprises ~500 m of marine carbonates and evaporites. The constant thicknesses observed in both the Rot (~100 m) and Muschelkalk Formations (~150 m) and the similar gamma-ray profiles, suggest tectonic quiescence. In well K15-02, the upper boundary of the Muschelkalk Formation marks the top of Triassic strata (Fig. 3).

4.4. Altena Group (Rhaetian to Oxfordian)

Towards the axis of the inverted anticline that dominates the study area, ~800 m of Altena Group strata are preserved conformably over the Keuper Formation of the Upper Germanic Trias Group (Figs. 3 and 4). Deep-water argillaceous shales were deposited in the Broad Fourteens Basin and are topped by Horizon H4 (Figs. 3, 4 and 5d). The brightest reflection on the interpreted seismic data is the Posidonia Shale — Horizon H3 (Fig. 5c). This horizon was not crossed by the interpreted wells. Significant individualisation of sub-basins and erosion associated with Mid-Kimmerian upwarping and Late Kimmerian I rifting caused the removal of Jurassic strata in the NE of the study area (Verweij and Simmelink, 2002). In addition, the first signs of raft tectonics occur in the Early Jurassic (Alves and Elliott, 2014), and a large listric fault offsets the strata in this unit, with thickness variations either side of the fault (Fig. 4). The top horizon (Horizon H4) of Unit I drapes over the raft and has little offset across the fault (Fig. 5d).

4.5. Schieland Group (Kimmeridgian to Valanginian)

The Schieland Group is a lensoidal package of rock bounded by Horizons H4 and H5 (Figs. 3 and 4). In the study area, these intervals are part of the Delfland Subgroup and contain carbonaceous claystones and thick-bedded sandstones belonging to the Breeveertien Formation (Van Adrichem Boogaert and Kouwe, 1993). They occur only within the crest of the inverted anticline (K15-07) and are thickest at the inversion axis (~710 m) (Fig. 6a–b). Both the upper and lower boundaries of the unit are unconformities. The lower boundary (Horizon H4) reflects the Late Kimmerian I rifting event and the upper boundary (Horizon H5) represents the Late Kimmerian II rifting event. Most faults located on the inversion crest displace these intervals, but rarely continue into the Altena Group. The unit is localised and does not occur to the SW in the salt-withdrawal basin, or NE towards the salt wall (Fig. 6). Importantly, all gas escape features in the study area are capped by Horizon H5 (Figs. 5e and 6). Morphologies and mechanisms for pipe termination are discussed in Section 6.

4.6. Rijnland and Chalk Groups (Valanginian to Danian)

The lower and upper boundaries of the Rijnland and Chalk Groups are regional unconformities. The base is the Late Kimmerian II unconformity (Horizon H5) and the top is the Base Tertiary unconformity (Horizon H6) (Figs. 2 and 5e–f). Deposition of coastal-shallow marine Vlieland Sandstone developed only in the basin axis. Calcareous claystones of the Vlieland Claystone Formation and marls of the Holland Formation (Rijnland Group) have a relatively constant thickness throughout the study area (~300 m and ~110 m, respectively) (Fig. 6). Deposition on the basin margins was sandier than in the basin centre as demonstrated by higher gamma-ray values in well K15-07 when compared to well K15-02 (Fig. 3). Unlike the strata below, the Ommelanden Formation (Chalk Group) is thicker away from the inverted anticline (~650 m) (Fig. 6). This is due to uplift being concentrated above the listric fault in the centre of the basin. Therefore, erosion during the Laramide and Pyrenean inversions removed more rock from the axis than the margin (Nalpas et al., 1995).

In the SW salt-withdrawal basin, concentric faults are nearly all concentrated in these units; few offset younger tertiary strata above horizon H6. On the inverted crest, concentric faults pass through into the Schieland Group, but rarely continue into Tertiary strata (Figs. 5f and 6a–c). No fluid pipes can be identified.

5. Analysis of fault families

Three fault families were identified and analysed in this work (Fig. 7). Listric faults constrained to Altena Group and Triassic units are associated with the gravitational gliding of individual rafts — isolated, fragmented blocks that are displaced over a décollement layer (Alves, 2012; Alves and Elliott, 2014; Penge et al., 1993). Shallower concentric faults occur within the salt-withdrawal basin and above the inversion crest. Comparisons are made between the three sets of faults.

Fault overlay diagrams display the geometry and spatial relationship between different faults (Fig. 7). Slices through different horizons have been stacked for each family and the largest gas pipes identified on the seismic data have been illustrated. One observation that can be drawn from this figure is the spatial relationship the shallow faults have with the deeper listric faults. There are two clusters of faults separated by 10–20 km of undeformed rock (Fig. 7). In the NE, crestal faults on the inverted anticline tend to dip towards the deeper listric fault, whereas in the SW, most salt-withdrawal basin faults dip away from the underlying listric fault. In both cases, the faults are concentrated on the convex side of the listric fault that is further away from the salt diapir. Faults on the inversion crest located furthest east curve away from the previously mentioned salt diapir (Fig. 7).

5.1. Faults in salt-withdrawal basin

Concentric faults in the salt-withdrawal basin are restricted to Cretaceous Rijnland/Chalk Groups and the earliest Tertiary Lower North Sea Group units. At the lower tips of these faults, throw values are negligible within the Rijnland Group, never cross-cutting horizon H5 (Figs. 6a–b and 8d–f). As a comparison, SW-dipping faults terminate above the Base Tertiary unconformity (Horizon H6). Throw-depth (*t-z*) plots reveal a distinct decrease in throw above H6, attributed to reactivation and upward propagation of the fault (Baudon and Cartwright, 2008) (Fig. 8d–e). Maximum throw (~20 m) is recorded towards the top of the Cretaceous Chalk Group, interpreted to be the locus of fault nucleation. Strata deformed by the first stage of faulting have been eroded by the inversion events, so the throw recorded above H6 must have been caused by renewed, post-inversion stresses. Both interpreted horizons and *t-x* plots show evidence of fault segment linkage as multiple peaks in throw maxima are observed (Fig. 9d–f) (Cartwright et al., 1995). Faults dipping SW are more numerous, but smaller conjugate NE dipping faults cut across the SW fault set. The concave side of the faults are focussed towards the salt diapir ~4000 m to the southwest (Fig. 1c).

5.2. Crestal faults on inverted anticline

Crestal faults on the inverted anticline are not truncated at H5 and displace Jurassic Schieland Group, Cretaceous Rijnland Group and the

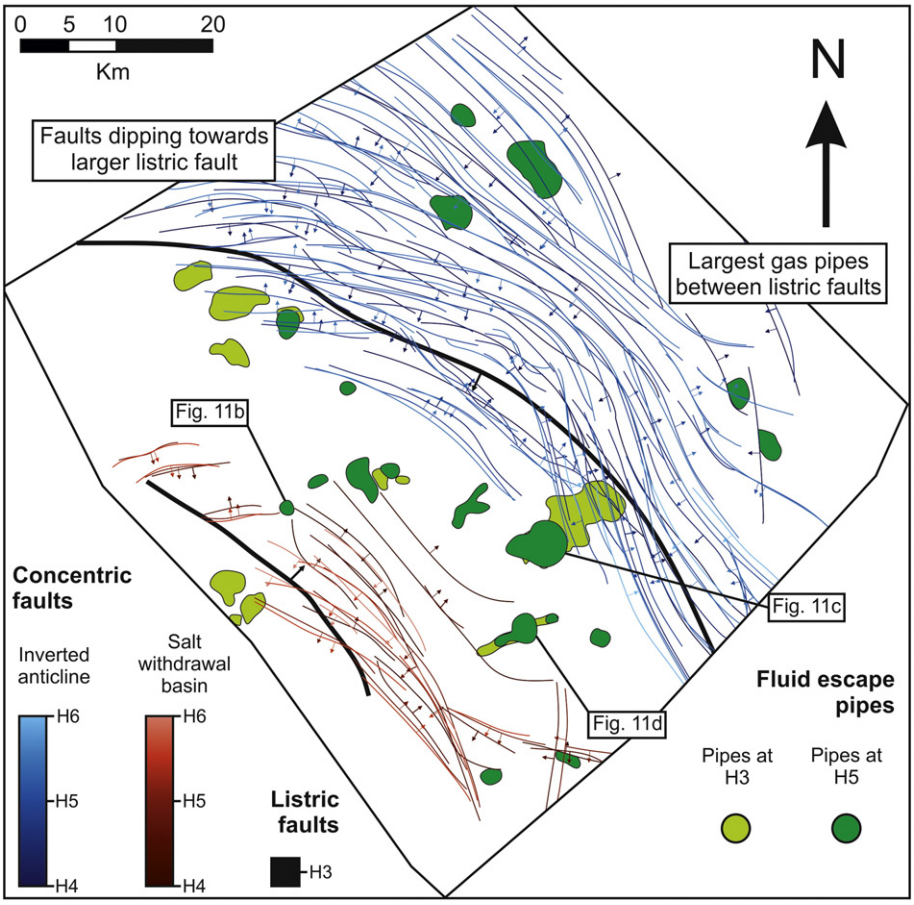

Fig. 7. Fault overlay diagram for all interpreted concentric faults. Faults were drawn from multiple reflections between Ommelanden Formation (Chalk Group) and the Delfland Subgroup (Schieland Group). Concentric faults in the salt withdrawal basin are shown in red, concentric faults on the crest of the inverted anticline are shown in blue, and listric faults are shown in black. Darker coloured faults indicate greater depth. Arrows show the dip direction of the fault. The morphology of gas pipes at their upper terminus (Horizon H5) and through Horizon *H3* arc drawn to show their spatial relationship to faults. Fluid escape pipes from Fig. 11a–c) at-c labelled.

Texel Formation of the Cretaceous Chalk Group, even though at the present day they occur at the same depth as the faults crossing the withdrawal basin (Fig. 8b–c). Crestal faults rarely propagate into Tertiary strata. Faults that do propagate above the Base Cretaceous Unconformity (H6) have throw values of <10 m (Fig. 8b–c). This figure shows that maximum throws (~35 m) are reached between the Chalk Group and the Rijnland Group.

Along H5 (Jurassic-Cretaceous boundary) there is a throw minimum, leading to another increase in throw down dip (Fig. 8c). This character reflects reactivation via dip linkage, where two separate faults have propagated towards each other (Baudon and Cartwright, 2008; Omosanya and Alves, 2014). Multiple throw peaks on *t-x* plots show fault segment linkage is a common process (Fig. 9b–c). With a dense mesh of faults occurring above the inversion crest, the fault traces are difficult to image, leading to inaccuracies in how the faults interact at this point. However, using variance slices and mapped horizons, it is clear that maximum curvature occurs at the top of the anticline and where many fault segments connect (Fig. 7).

5.3. Listric faults

Listric faults are less common in the study area and bound individual Triassic-Jurassic rafts (Alves and Elliott, 2014). These faults sole-out in the Zechstein Salt, which acts as a décollement layer. Along strike, single listric faults are linked to multiple fault segments on the inverted anticline (Fig. 10). Where the lower tips of the crestal faults join to the upper tip of the listric fault (H4), throw decreases from ~100 m to ~30 m (Fig. 8a). This sudden jump in throw values suggest the listric fault was reactivated with the multiple crestal fault segments connecting to the listric fault, providing evidence that reactivation caused vertical propagation via dip linkage. Two sudden gradient changes occur on *t-x* plots of listric faults where throw increases by ~300 m. Three fault segments are highlighted in Fig. 9a, each separated by a trough in the along strike throw profiles. Maximum displacement along this fault is observed at its SE tip, where the fault intersects a salt wall (Figs. 1c and 9a). The fault does not continue on the east side of the salt wall, suggesting the movement of salt has influenced the variations in along strike displacement. Thickness variations between the footwall and the hanging-wall of the listric faults show they are syn-sedimentary (Childs et al., 2003).

6. Evidence for fluid expulsion

Highly localised vertical to sub-vertical pathways of focused fluid flow (fluid escape pipes) are seen on seismic data as columns of disrupted reflection continuity (Cartwright and Santamarina, 2015;

Fig. 8. Throw-depth (*t-z*) profiles for six representative faults. Unconformity surfaces relating to points of reactivation and linkage are highlighted with a dashed line. Multiple throw maxima on a single plot provides evidence of reactivation along a fault (Baudon and Cartwright, 2008). Colours used represent the units identified in Fig. 3. a) — listric fault; b–c) — inverted anticline fault; d–f) — salt withdrawal basin fault.

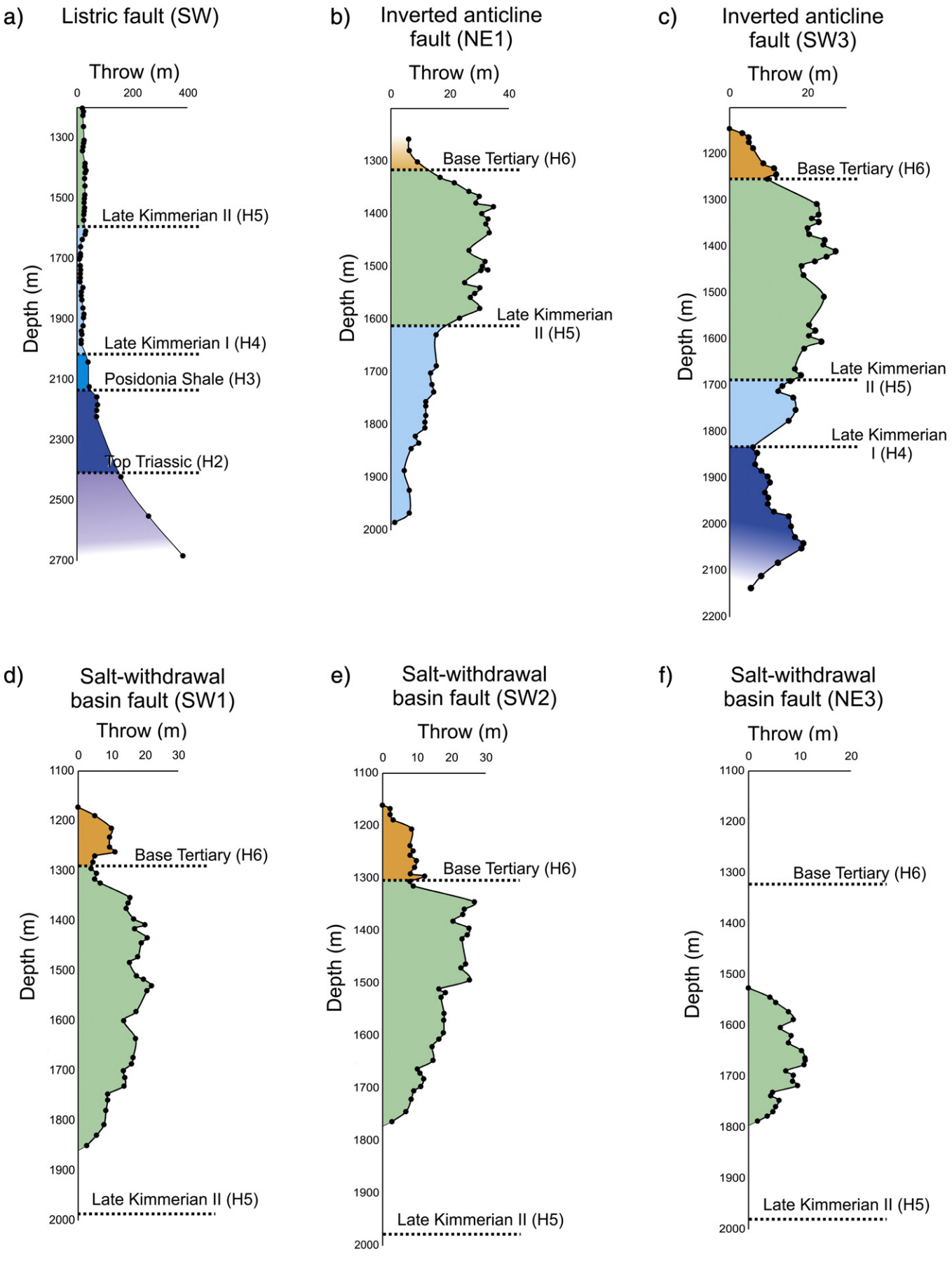
a)
Listric fault (SW)
Throw (m)
0
200
400
Depth (m)
1300
1500
1700
1900
2100
2300
2500
2700
Late Kimmerian II (H5)
Late Kimmerian I (H4)
Posidonia Shale (H3)
Top Triassic (H2)
b)
Inverted anticline fault (NE1)
Throw (m)
0
20
40
Depth (m)
1300
1400
1500
1600
1700
1800
1900
2000
Base Tertiary (H6)
Late Kimmerian II (H5)
c)
Inverted anticline fault (SW3)
Throw (m)
0
20
Depth (m)
1200
1300
1400
1500
1600
1700
1800
1900
2000
2100
2200
Base Tertiary (H6)
Late Kimmerian II (H5)
Late Kimmerian I (H4)
d)
Salt-withdrawal basin fault (SW1)
Throw (m)
0
10
20
30
Depth (m)
1100
1200
1300
1400
1500
1600
1700
1800
1900
2000
Base Tertiary (H6)
Late Kimmerian II (H5)
e)
Salt-withdrawal basin fault (SW2)
Throw (m)
0
10
20
30
Depth (m)
1100
1200
1300
1400
1500
1600
1700
1800
1900
2000
Base Tertiary (H6)
Late Kimmerian II (H5)
f)
Salt-withdrawal basin fault (NE3)
Throw (m)
0
10
20
Depth (m)
1100
1200
1300
1400
1500
1600
1700
1800
1900
2000
Base Tertiary (H6)
Late Kimmerian II (H5)

Gay et al., 2007; Hustoft et al., 2007). The locations of pipes are often controlled by underlying structures such as fault zones, salt diapirs, erosional surfaces or anticlinal crests (Gay et al., 2007). Fluid escape pipes are generally clustered (Cartwright and Santamarina, 2015; Gay et al., 2007; Hustoft et al., 2010). Within the studied polygon, 14 clusters of 109 individual pipes (clustered and non-clustered) were measured (Fig. 7). The upper terminus of individual pipes range in width from ~200 m to ~1200 m, whereas their height depends on the depth of the root zone and ranges from ~300 m to ~1100 m. Most of the gas pipes are rooted in the Lower Germanic Trias Group, crossing the Posidonia Shale (Fig. 11). All the gas pipes terminate at the Jurassic-Cretaceous boundary (Horizon H5-Late Kimmerian II rifting event) (Figs. 5d–e, 6b–c and 11).

Different morphologies of the upper terminus of fluid escape pipes are observed in Figs. 5d, 7 and 11. All are circular to slightly elliptical in planform, but are characterised by variations in the shape in cross-section and size. Strata above and within fluid escape pipe a) have been upwarped to form a mound (Fig. 11a). Reflections above H5 are also mostly continuous across the pipe, maintaining their thickness and not onlapping the structure (Fig. 5a).

In Fig. 11b, fluid escape pipe b) is small compared to other examples and is strongly elliptical in planform. There is no topographic expression above H5, although reflections thin out towards the upper terminus of pipe b), indicating numerous stages of growth and pulses of fluid flow. Fluid escape pipe c) has the same shape as mud volcanoes described in Kopf (2002) (Fig. 11c). Reflections onlap the flanks both within and outside the structure. It tapers to a root zone within the Lower Germanic Trias Group, ~100 m above a small salt swell. Above H5, topographic relief has caused sediments to onlap onto the SE flank and thin over the crest of the structure. Fluid escape pipe d) is a cluster of smaller individual pipes (Figs. 7 and 11d). They each show examples of buried pockmarks (Andresen and Huuse, 2011; Cartwright and Santamarina, 2015). The pipes root into the Zechstein Salt, disrupting reflections in H1. The geometry of the upper terminus is consistent with those described by Andresen and Huuse (2011) as depressions, interpreted as pockmarks, having erosional bases and onlapping fill.

7. Slip tendency analyses for concentric faults

7.1. Slip tendency results and effects of changing pore fluid pressure

Due to the curvature of the concentric faults, some sections of the fault surfaces may be optimally oriented for reactivation in the modern stress field. Slip tendency analyses demonstrate how the likelihood for a fault to fail can change along the strike of a curved concentric fault (Fig. 12). The results calculated on Move™ are provided as a value normalised to the maximum slip: $\overline{T}_s = T_s/T_{max}$, so that 1 indicates the highest expected level of slip and 0 is no slip (Healy et al., 2015). This allows direct comparisons between different sets of results (Healy et al., 2015; McFarland et al., 2012). Fault models in Fig. 12 show slip tendencies on the fault surfaces and include the orientations of principal stresses. Maximum normalised slip tendency values occur on sections of the fault that strike 30° to the orientation of σ_1. When $P_f = 0$ MPa, segments of faults in the north striking 30° to σ_1 have $\overline{T}_s$ values approaching 0.2, whereas in the south, the faults segments are striking <30° to σ_1 and have $\overline{T}_s \geq 0$ (Fig. 12a). Relatively high slip tendencies are also observed in shallower faults with lower dips, as fault reactivation in a compressional setting favours low-angle thrusts (Wiprut and Zoback, 2002). Smaller faults in the SW salt-withdrawal basin have higher $\overline{T}_s$ values than faults on the inverted anticline and listric faults as they are an ideal orientation for fault reactivation. They are generally smaller and less curved, and hence the slip tendency is more homogeneous along strike (Fig. 12). Along these sets of faults, a zone of high $\overline{T}_s$ values occur on faults that strike ~295°, 30° to the orientation of σ_1 and optimal for strike-slip reactivation (De Lugt et al., 2003; Nalpas et al., 1995).

We plotted Mohr circles to help visualise and quantify how increasing pore fluid pressure reduces the effective normal stress (σ_n'), therefore increasing the $\overline{T}_s$ moving the fault towards failure (Fig. 13a). Two Coulomb failure envelopes have been plotted on this diagram to show the conditions required to reactivate a fault (fault failure) or create new faults in an intact rock (intact rock failure). An average fault depth of 1500 m was considered and boundary conditions for the angle of internal friction (φ) and cohesion (C) of 30° and 10 MPa were used respectively (Barton, 1973). The same angle of internal friction was assumed for fault reactivation, but cohesion was set to 0 MPa (Morris et al., 1996).

The assumption of a cohesionless surface for the fault plane does not represent a true fault surface. All faults will have some amount of roughness, a character that increases the amount of friction expected on fault surfaces (Barton, 1973). However, approximating a cohesionless fault will give the lowest boundary for failure along a fault plane. These failure envelopes allow us to predict optimum fault orientations for reactivation by measuring the angle between σ_1 and the point of intersection between the envelope and the Mohr circle (2θ). The fault strike where reactivation is likely to occur is consequently 90–($\theta/2$). The Mohr circle in Fig. 13a at 25 MPa intersects the fault failure envelope between 103.5° and 136.5° from σ_1. This indicates that faults striking at ~21.75°–38.25° to σ_1 are most likely to fail, matching the results found on the fault models. As pore fluid pressure is increased to 30 MPa, optimum angles for reactivation are extended to ~3.5°–56.5° to σ_1. This is emphasised by the fault models in Fig. 12c and d, where at 30 MPa, anything above the fault failure envelope has a $\overline{T}_s \approx 1$.

7.2. Slip tendency analysis using different lithologies

To help understand the behaviour of different sets of concentric faults, representative Mohr circles have been created for key lithologies. Measurements of φ and C for each lithology were taken from Farmer and Jumikis (1968). Fig. 13b shows Mohr circles for the faults within the salt-withdrawal basin. The average depth of these faults is ~1600 m, and the most common lithology they displace is chalk. As in Section 7.1, two failure envelopes were added to the diagrams; $\varphi = 39°$ for both, and C = 3.5 MPa for the failure within the intact rock and 0 MPa for fault reactivation. Results show that faults are only likely to reactivate when pore fluid pressures reach 30 MPa and the fault strikes ~11.5°–40° relative to σ_1. New faults are not expected to form under these conditions. Concentric faults on the inverted anticline have an average depth of ~2000 m and cut into the Vlieland Sandstone, a small but important reservoir rock. A cohesion value of 8 MPa and a φ value of 35° was calculated for a sandstone (Farmer and Jumikis, 1968). Between pore fluid pressures of 0 MPa and 30 MPa, $\overline{T}_s$ never exceeds 0.5 (Fig. 13c). Even when pore fluid pressures reach 30 MPa, the Mohr's circles do not pass the fault failure envelope, indicating that faults are unlikely to reactivate under these conditions (C = 0 MPa).

The height of the listric faults is >1 km, so the Posidonia Shale was chosen as a representative horizon, as it is a prolific source rock in the Southern North Sea (Duin et al., 2006). The average depth of the Posidonia Shale is 2400 m and predicted C and φ are 3 MPa and 15° respectively (Farmer and Jumikis, 1968). Such a low angle of internal friction means that an increase in P_f greatly increases the chances of fault reactivation. At 25 MPa, faults oriented between 21° and 54° to σ_1 are likely to reactivate (Fig. 13d). When $P_f = 30$ MPa, not only are faults striking 15.5°–59.5° to σ_1 likely to fail, but new faults striking 31.5°–43.5° to σ_1 start to form.

8. Discussion

8.1. Propagation history of concentric faults

The throw profiles in Figs. 8 and 9 help determine the timing of fault initiation. In the study area, it is not possible to infer the exact age of

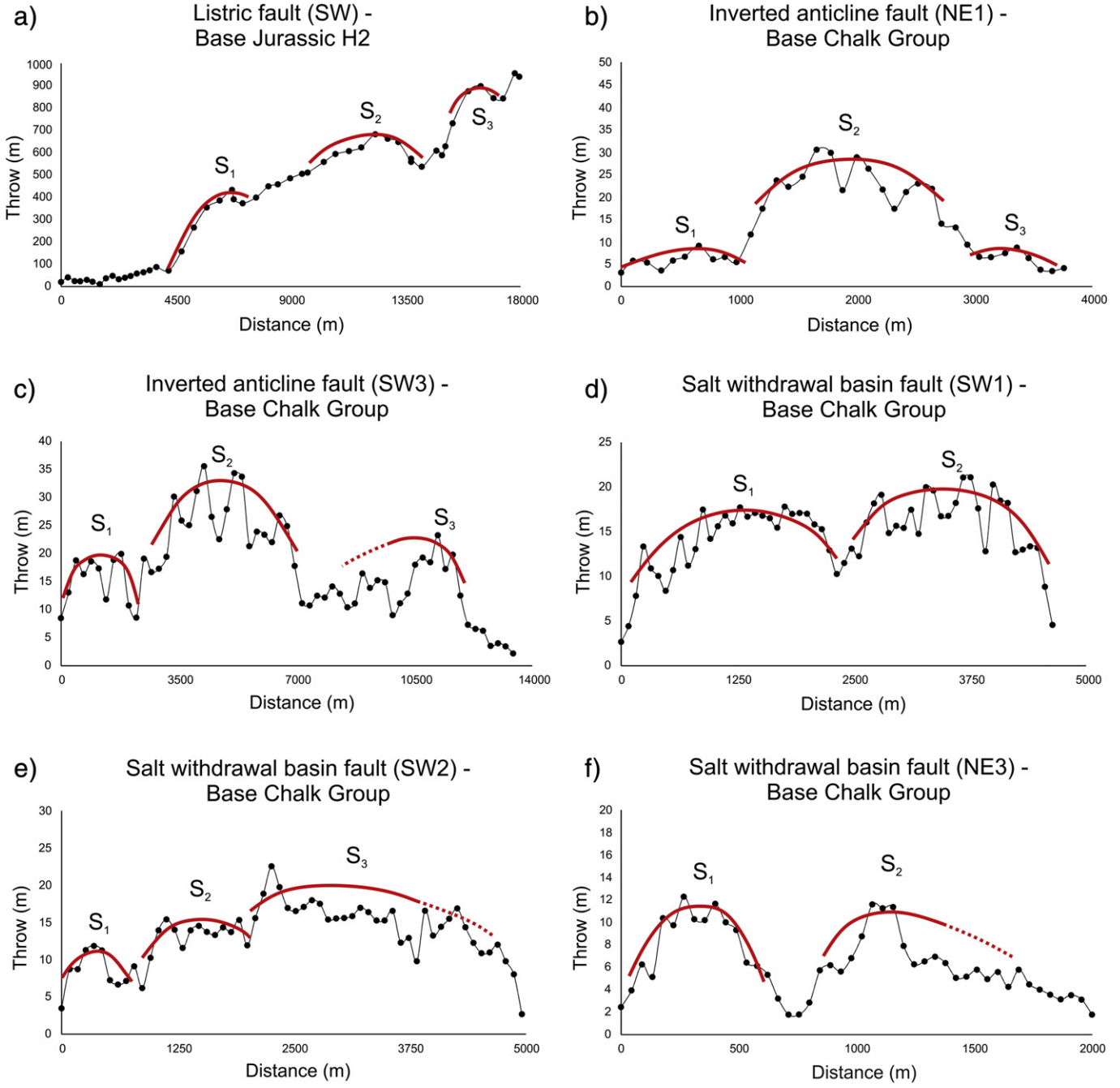

Fig. 9. Throw-distance (*t-x*) profiles of the same faults analysed in Fig. 8. Multiple peaks in throw values indicate different fault segments, as highlighted by the red lines and corresponding labels S_1, S_2 and S_3 (Cartwright et al., 1995). Concentric faults on the inversion crest and in the salt withdrawal basin show the most obvious segment linkage, but listric faults have stepped profiles as the throw suddenly increases with the addition of a new segment towards the salt wall in the east. a) — listric fault; b–c) — inverted anticline fault; d–f) — salt-withdrawal basin fault.

fault initiation, but chronological boundaries can be estimated for the interpreted fault families. Fig. 14a–d shows a schematic evolution of the study area, highlighting the ages for concentric fault formation.

Faults generated in salt-withdrawal basins occur only above Horizon H5. The unconformity H6 truncates faults, so their formation must have occurred prior to the erosion of Chalk Group units at the end of the Cretaceous. The faults appear to be blind as there is no growth of strata across them. Normal offset and steep dips of the faults imply that they must have formed during an extensional phase, the most recent being prior to the Laramide inversion (Verweij and Simmelink, 2002).

Faults on the inversion crest have maximum throw values in the Rijnland Group of Early Cretaceous age, displacing older strata than faults in the salt-withdrawal basin. The faults on the inversion crest have steep dip and normal offset, similar to the faults in the salt-withdrawal basin, indicating extensional forces were acting upon them. However, results indicate faults formed during the Late Cretaceous, which was dominated by reverse movement along low-angle thrust faults. Fig. 7 hints at a spatial relationship between inversion crest/salt-withdrawal basin faults formed in the Cretaceous and listric faults forming through the Triassic and Jurassic. Possible mechanisms for the formation of concentric faults on the inversion crest and in the salt-withdrawal basin are:

- Using the Zechstein salt as a detachment layer, raft bounding faults were reactivated during discrete tectonic pulses. Bending and differential subsidence of strata draping these faults could have allowed

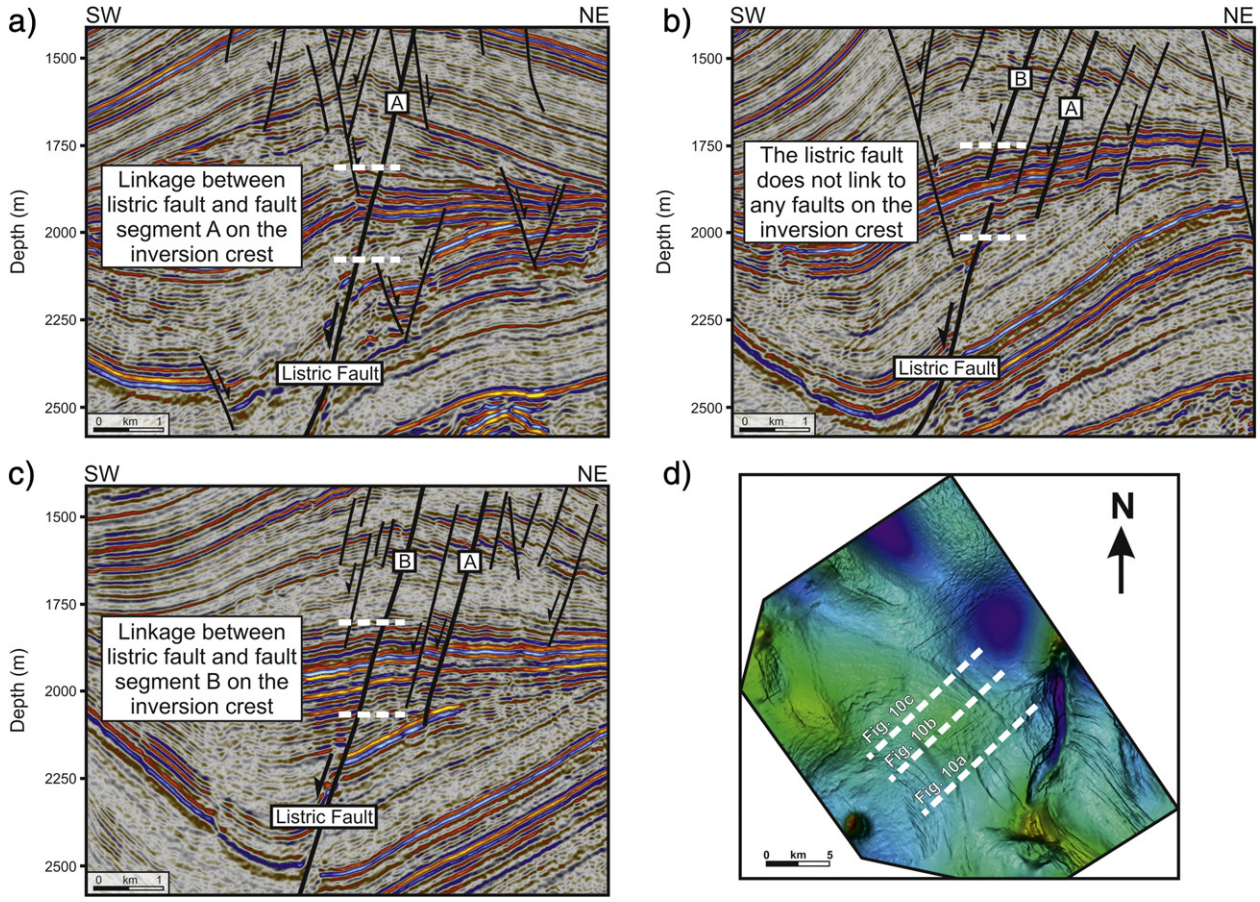

Fig. 10. Seismic lines depicting how the raft-bounding listric faults propagate upwards and link with segments of faults on the inverted anticline. White lines represent the area of connection between the listric fault and faults on the inverted anticline. Fault segment A connects to the listric fault on the SE of the anticline (a), and then disconnects in the centre (b). Fault segment B then connects to the listric fault on the NW side of the anticline (c), whilst the tipline of segment A does not join to the listric fault. d) shows the locations of a, b. and c.

extensional failure over the edge of the footwall block (De Lugt et al., 2003; Oudmayer and De Jager, 1993) (Fig. 14c).

- Halokinesis in the Southern North Sea occurred from the Late Triassic onwards. During the three inversion events, salt was squeezed through older reactivated faults, being withdrawn from within the basin (Coward and Stewart, 1995). Thus, extensional faulting developed as secondary rim synclines formed, bending the strata towards the subsiding minibasin adjacent to the salt diapir (Fig. 14c) (Coward and Stewart, 1995; Maione and Pickford, 2001; Nalpas et al., 1995). Maione and Pickford (2001) described the geometry of the extensional faults reflecting that of the salt diapir which explains how the whole length of the concentric fault experiences normal offset.

Although the relative timing of initiation between these faults is unknown, it is postulated that both mechanisms were involved in forming the different faults. All faults were reactivated during the Early Tertiary (Fig. 14d). Salt-withdrawal basin and crestal faults cross the Base Tertiary Unconformity (H6) and have a typical reactivated *t-z* profile with a stepped gradient, suggesting upward propagation during reactivation (Baudon and Cartwright, 2008). Reactivation of inversion crest faults and listric faults connecting the two families appears to be caused by dip linkage (Figs. 8a and 10), with throw maxima separated by a throw minimum (Baudon and Cartwright, 2008). Extensional faults (dipping at ~60°) would be hard to reactivate with reverse-slip. In many settings it is easier to form new, low-angle thrusts behind the normal fault than reactivate it. Without the presence of low-angle thrust faults (and stress orientations <30° to the fault strike) these faults are considered to have reactivated obliquely (De Lugt et al., 2003; Hooper et al., 1995). Transpressional or transtensional forces may have acted on parts of the concentric faults, but no structures are observed to provide evidence for this.

Lateral propagation of fault segments may have increased the curvature of the faults. Though it is hypothesised that the concentric faults formed due to differential subsidence or salt-withdrawal, fault segment-tips may have propagated along a curved path and intersected the next fault. This curvature is due to the influence of the nearby fault on the stress field of the propagating fault (Ferrill et al., 1999). This would explain why, in the NW of Fig. 7, smaller segments curve into larger faults.

8.2. Timing of pockmark and fluid pipe formation and their relation to concentric faults

It is important to understand fluid expulsion processes because they can be primary or secondary pathways for hydrocarbon migration through a sedimentary basin, potentially by-passing a seal unit (Cartwright et al., 2007; Cartwright and Santamarina, 2015). Carbon sequestration and CCS efforts could be hindered by fluid escaping through the overburden, with evidence for such events occurring in the Sleipner pilot project (Arts et al., 2004; Cathles et al., 2010).

The morphology of the upper termination of fluid escape pipes aids in determining its timing of formation (Andresen and Huuse, 2011; Cartwright and Santamarina, 2015; Hustoft et al., 2010; Løseth et al., 2009; Van Rensbergen et al., 2007). Examples of past movement is described and interpreted in this section from the seismic data. Multiple

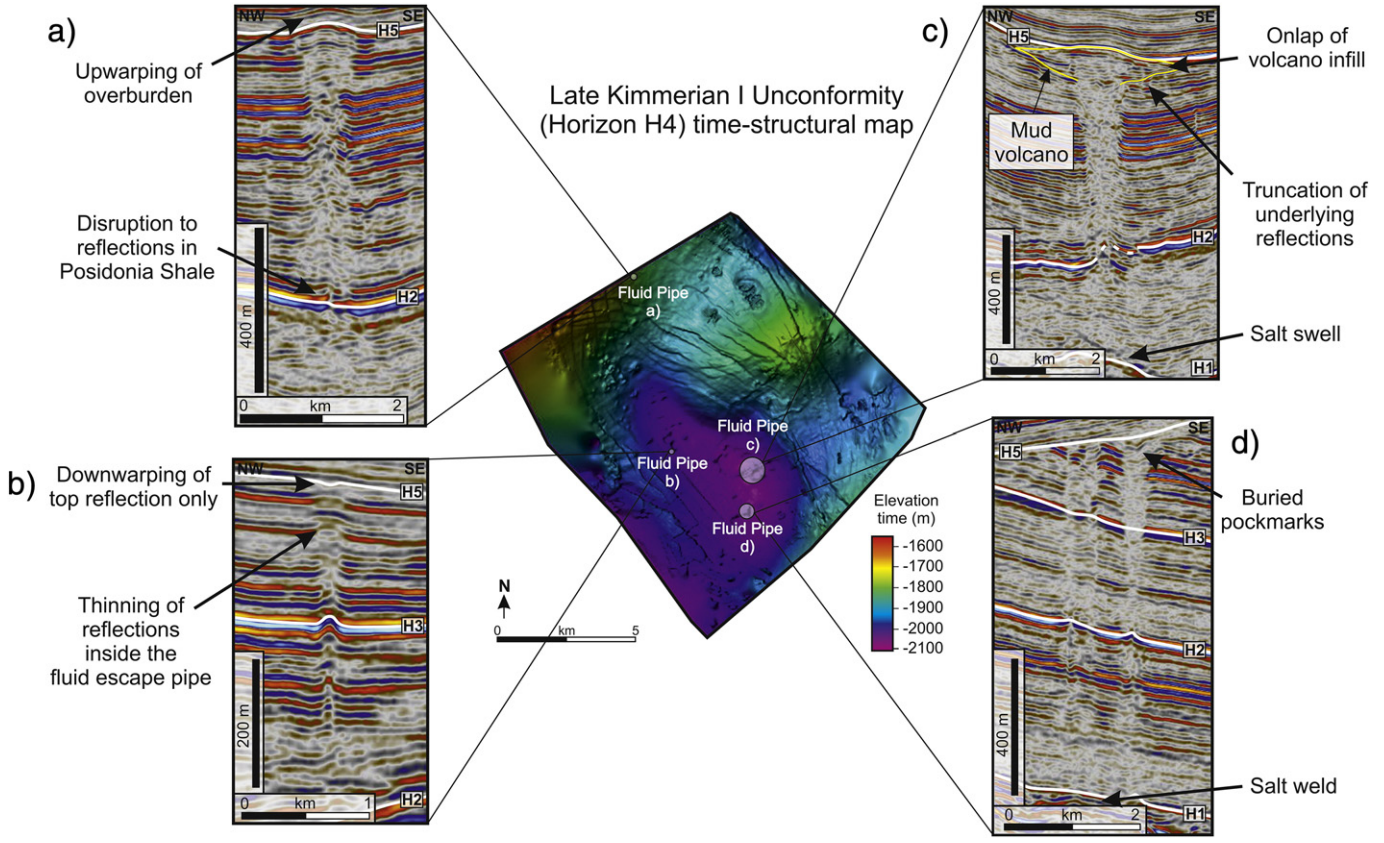

Fig. 11. Seismic character of fluid escape pipes in the study area. Each diagram (fluid pipe a–d) has a seismic slice showing the fluid pipe and relevant features. All the fluid pipes terminate at H5 and are sourced deeper than the Jurassic units. a) Upwarped reflections above the fluid pipe in the form of a mound. There is no thinning on these horizons, indicating sediment was deposited before fluid escape occurred. b) A small fluid pipe with downwarped reflections at the upper terminus. Thinning of reflections below H5 suggests multiple stages of growth. c) A mud volcano is distinguishable at the tipper terminus of the fluid pipe. The salt swell indicates the fluid is sourced below the Triassic units. d) A cluster of fluid pipes that have buried pockmarks and pipes rooting to the Zechstein Salt (H1).

phases of fluid flow are hard to analyse, as each new migration event obscures previous seismic evidence of fluid flow (Cartwright and Santamarina, 2015). Mud volcanoes and pockmarks are both topographic features that formed at the surface. In a pockmark, basin fill onlaps underlying rocks, whereas sediments onlap the flanks of a topographically elevated mud volcano (Andresen and Huuse, 2011; Kopf, 2002). Thinning of reflections over high relief structures (mud volcanoes/mounds) is another indication of palaeo-fluid flow. Upwarping of the overburden indicates that sediment had been deposited and buried before the fluid escape pipe formed (Frey-Martinez et al., 2007). Fluid pipes may terminate at boundaries that prevent them from propagating vertically, instead diffusing horizontally into a more permeable reservoir (e.g. Schieland Group) (Cartwright and Santamarina, 2015; Hustoft et al., 2007).

Overpressured conditions are often a prerequisite for generating fluid escape pipes. In general, Rotliegend reservoirs in the Broad Fourteens Basin are currently hydrostatic (Verweij and Simmelink, 2002). Overpressured conditions last occurred in the Late Jurassic when sedimentation rates were exceptionally high (Osborne and Swarbrick, 1997; Verweij and Simmelink, 2002). Fluid escape features described in Section 6 terminate at the Jurassic-Cretaceous boundary, coinciding with Late Jurassic overpressure (Osborne and Swarbrick, 1997). Most of the pipes in the study area are rooted below the Lower Germanic Trias Group, either from the Main Buntsandstein Formation or the Rotliegend Sandstone. Very few pipes root at the Posidonia Shale indicating that hydrocarbons in the fluid pipes were largely fed by gas sourced from Carboniferous coal.

According to Verweij et al. (2003) peak Carboniferous gas expulsion and migration occurred in the Early Cretaceous pre-inversion time. Breaching of the Zechstein seal during inversion allowed vertical escape of gas towards Vlieland Sandstones. The morphologies of pipes and generation of Carboniferous gas point towards concentrated fluid flow syn-rift/pre-inversion, prior to formation of concentric faults. Reactivated faults on the crest of the inverted anticline may have leaked gas out of the reservoir that was charged by flow along deeper listric faults during inversion.

Slip tendency data indicate that the greatest amount of slip will occur in vertical channels (Fig. 12). Discrete, vertical patches of high slip tendency coincide with the formation of fluid escape pipes above the listric faults. Fig. 7 shows the escape pipes mainly clustered between the two listric faults. This diagram only shows the faults at a single horizon, although the arrows indicate the faults dipping below base of the fluid escape pipes. Large vertical pipes can also be seen rising from base of the listric faults in Fig. 6b and c. Pipe-like fluid flow is more conductive than flow along a planar surface (Blenkinsop, 2004). The combination of vertical fluid pipes associated with concentric faults and vertical patches of high slip tendency indicates that the whole length of the fault does not need to reactivate for it to be able to transmit fluid through a seal rock. Due to the high degree of segmentation, optimally oriented patches of the fault may fail and transmit fluids, whilst other parts of the fault remain inactive.

8.3. Implications for CCS and EOR

Both CCS and EOR require injection of high pressured fluids into the subsurface. This study explores the possibilities of CO_2 storage in post salt reservoirs and recovering unconventional oil from Posidonia Shale. Current efforts into the capture and storage of CO_2 offshore Netherlands include the P18-4 gas field ROAD (Rotterdam Capture and Storage Demonstration) Project, which is planning to store ~5 Mt

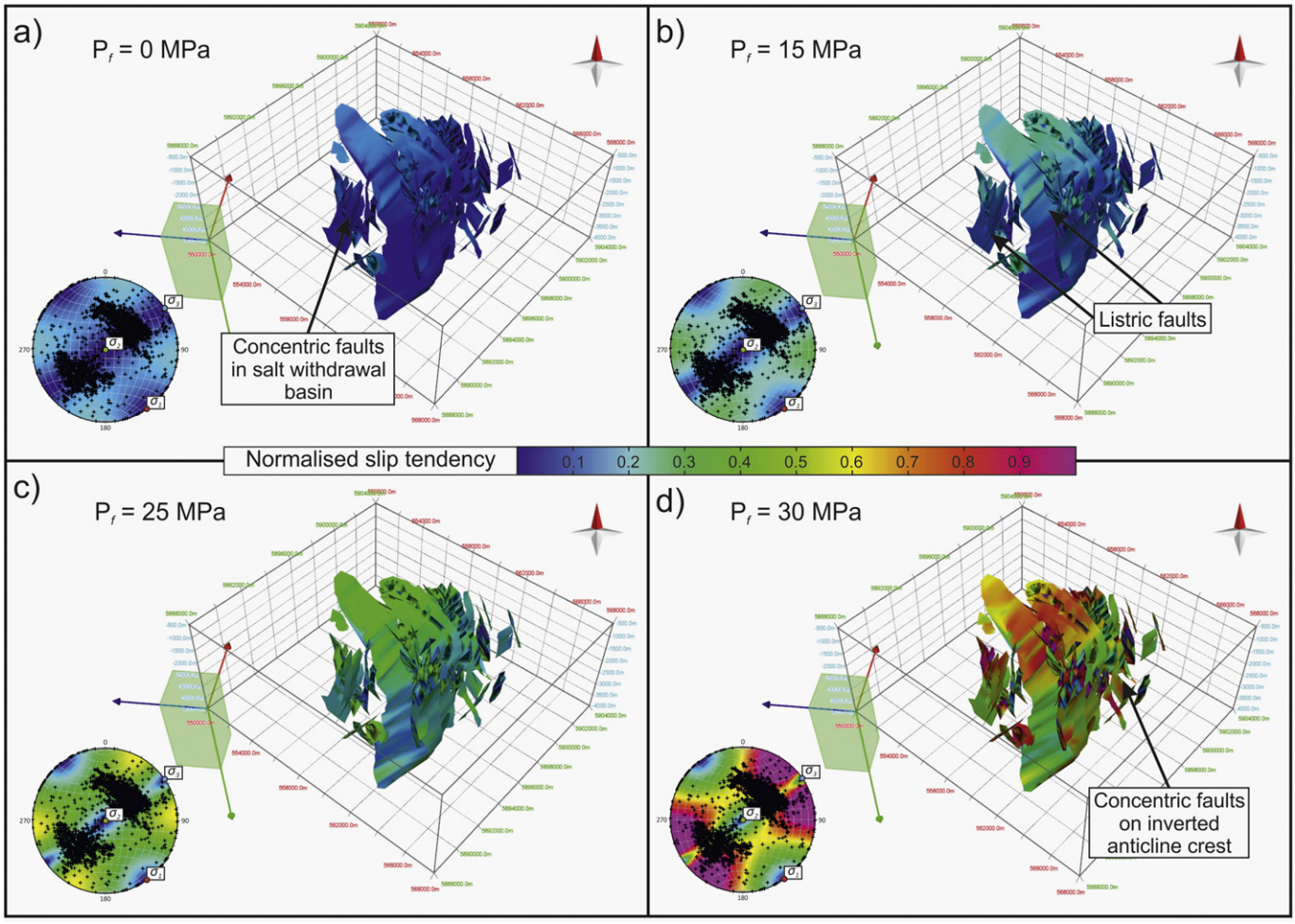

Fig. 12. Normalised results of slip tendency analyses overlain onto fault models. Red/pink represents high chances of slip, whereas blue/turquoise represent low chances of slip. Pore fluid pressure (P_f) increase causes an increase in slip tendency. a–d) represent P_f of 0 MPa, 15 MPa, 25 MPa and 30 MPa respectively. Stereonets compliment each slip tendency diagram showing the poles to the planes as black dots.

CO_2 in the Main Buntsandstein Subgroup over 5 years (Arts et al., 2012). Injection pressures are expected to be maintained at 35 MPa for the duration of the project.

At an average fault depth of 1500 m, pore fluid pressures of 25 MPa are sufficient to induce slip on optimally oriented fault surfaces; at 30 MPa, most fault orientations will likely fail. The Vlieland Sandstone (a possible reservoir for CO_2 storage) is competent and faults are unlikely to reactivate even at $P_f = 30$ MPa, whereas in shales at 2400 m depth, new faults can form at $P_f = 30$ MPa (Fig. 13). These estimates are only representative of the main lithologies considered. With a resolution of ~10 m, small scale lithological changes are highly likely and will influence the C and φ.

Fault segmentation is common in this part of the Southern North Sea. The degree of segmentation in this area increases the variability of fault orientation along strike (Fig. 7). Leveille et al. (1997) discussed the relationship between orientation, timing and magnitude of deformation relative to faults and their sealing ability. Thus, segmented concentric faults will have different sealing abilities along the horizontal fault trace (Kattenhorn and Pollard, 2001). When injecting CO_2 into reservoirs that are compartmentalised by fault segments, the pore fluid pressure may increase in a single compartment, but not in other compartments (Kattenhorn and Pollard, 2001; Leveille et al., 1997). Therefore the slip tendency would depend on where the gas was being injected. The model presented in this work does not take into account the compartmentalisation of the reservoir, which could have major implications on the slip tendency and thus the location of CO_2 injection.

Alternatively, the locus of fault segment linkage may increase the permeability of the rocks. Where the fault segments interact, active fracturing provides a pathway for fluids (Curewitz and Karson, 1997). The highest concentration of fault-segment linkage is in the low permeability Rijnland and Chalk Groups (Figs. 5e and 7), which are the expected seal units for the Delfland Subgroup and Vlieland Sandstone reservoirs (Bouw and Essink, 2003). Though these faults occurred after the fluid pipe generation, future vertical migration of fluid through the interaction zones is possible if there is any of reactivation along the fault whilst injecting CO_2. Concern for failure of seal cutting faults during pore fluid pressure increases may explain why no wells have been drilled into, or south of, the inverted anticline.

9. Conclusions

The main conclusions of the study are:

a) Concentric faults with a normal offset developed contemporaneously with regional compression. Local stresses did not represent the overall stress regime in the Southern North Sea during their evolution. One set of faults adjacent to the salt diapir formed in response to local extensional stresses. Salt was withdrawn around the diapir and a rim syncline started to subside, creating new extensional faults as the strata bent into the minibasin. Concentric faults on an inversion anticline are closely related to deeper raft bounding faults, with differential subsidence creating extension about the raft boundary.

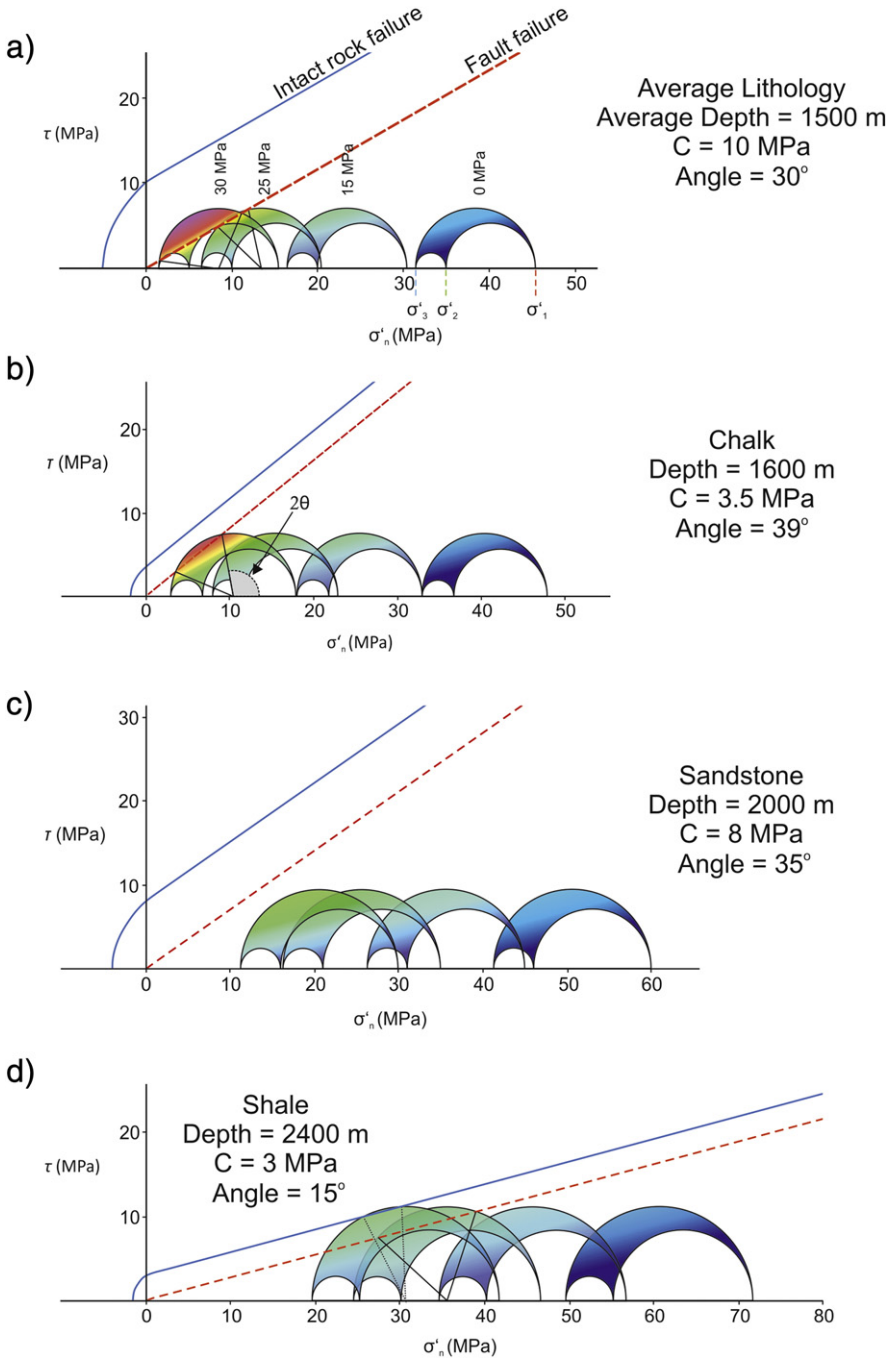

Fig. 13. Mohr's circle diagrams of different lithologies in the study area and the effects of increasing pore fluid pressure. a) Diagram demonstrating how increasing the pore fluid pressure makes a fault more likely to reactivate. An average depth and lithology was assumed for the parameters. b–d) Diagrams showing the likelihood for faults to reactivate in the Chalk Group, Vlieland Sandstone and Posidonia Shale respectively. Values of cohesion (C) and angle of internal friction (p) were calculated by Farmer and Jumikis (1968).

b) Growth histories of concentric faults can be complex, with vertical linkage from multiple phases of reactivation during inversion and horizontal segment linkage via lateral propagation. Fault segment linkage can increase the curvature of faults as each segment curves towards the propagating larger fault.

c) Slip tendency analyses shows patches of high slip along parts of the fault that are optimally oriented with respect to the present day stress field, increasing the chances of fluid leakage. The heterogeneity of fault slip along strike increases with the length and curvature of a fault, making evaluation of each individual fault necessary. Sub-vertical patches of high slip tendency along a single fault occur near vertical fluid pipes. Variations in lithology and depth of faults have a strong influence on the slip tendency and the failure profiles. Even at depth, faults cross-cutting the Posidonia Shales are much more likely to reactivate than those within shallower sandstones as pore fluid pressure increases.

d) Fluid escape features found on 3D seismic data provide evidence for vertical migration of fluids from Carboniferous Gas reservoirs. Overpressured conditions in these reservoirs occurred most recently during the Late Jurassic allowing fluid to flow to the surface and form pockmarks and mud volcanoes, indicating that most fluid pipes are palaeo-features.

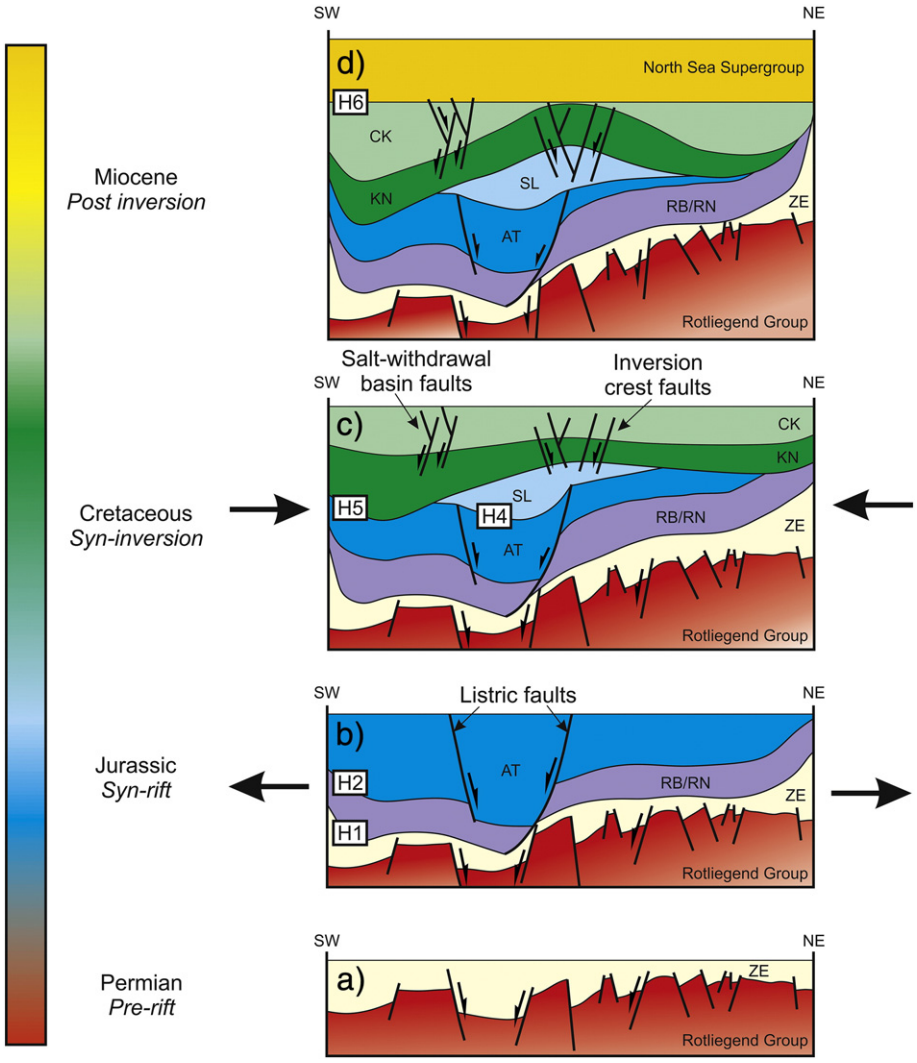

Fig. 14. Schematic cartoon of the geological evolution of the study area (based on Fig. 6) highlighting the age and growth of different fault families. The cartoon shows listric faults active in during the Jurassic syn-rift form in association with rift-raft tectonics. Shallower concentric faults are formed by the Late Cretaceous in response to the evacuation of salt (salt-withdrawal) and differential subsidence of the footwall of a listric fault (faults on the inversion anticline crest). ZE, Zechstein Group; RB, Lower Germanic Trias Group; RN, Upper Germanic Trias Group; AT, Altena Group; SL, Schieland Group; KN, Rijnland Group; CK, Chalk Group.

e) In the inversion crest, where the Vlieland Sandstone reservoir is still preserved, concentric faults cut through the strata and create a pathway for fluids to leak. Faults are unlikely to reactivate at pore fluid pressures <30 MPa in the sandstones, however, they may reactivate within the chalk seal above. Although faults may provide pathways to fluid flow, they can also compartmentalise a reservoir. If this is the case, then an increase in pore fluid pressure on one fault might not have the same effect the other side of the fault.

f) Storage of CO_2 in Block K15 is possible at pore fluid pressures similar to those being implemented in the Southern North Sea (Arts et al., 2012). To ensure no faults are reactivated and transmit fluids, pore fluid pressures will have to remain <30 MPa. Faults studied here are highly segmented, and the locus of segment interaction can provide a suitable pathway for seal bypass.

Acknowledgements

The work contained in this paper was conducted during a PhD study undertaken as part of the Natural Environment Research Council (NERC) Centre for Doctoral Training (CDT) in Oil & Gas and is funded by NERC and co-sponsored by Cardiff University, whose support is gratefully acknowledged. We thank Tullow Oil for access and permission to publish examples from their 3D seismic data volumes. Schlumberger (for Petrel©) and Midland Valley (Move™) are acknowledged for the provision of academic licences to Cardiff's 3D Seismic Lab. NLOG and TNO are acknowledged for the well data in this work. We thank two anonymous reviewers and the editor J. Crider for their constructive comments.

References

Alsop, G.I., 1996. Physical modelling of fold and fracture geometries associated with salt diapirism. Geol. Soc. Lond., Spec. Publ. 100, 227–241.

Alves, T.M., 2012. Scale-relationships and geometry of normal faults reactivated during gravitational gliding of Albian rafts (Espírito Santo Basin, SE Brazil). Earth Planet. Sci. Lett. 331, 80–96.

Alves, T.M., Elliott, C., 2014. Fluid flow during early compartmentalisation of rafts: a North Sea analogue for divergent continental margins. Tectonophysics 634, 91–96.

Anderson, E.M., 1951. The Dynamics of Faulting, 1951. Oliver and Boyd, Edinburgh.

Andresen, K.J., Huuse, M., 2011. 'Bulls-eye' pockmarks and polygonal faulting in the Lower Congo Basin: relative timing and implications for fluid expulsion during shallow burial. Mar. Geol. 279, 111–127.

Arts, R., Eiken, O., Chadwick, A., Zweigel, P., van der Meer, B., Kirby, G., 2004. Seismic monitoring at the Sleipner underground CO_2 storage site (North Sea). Geol. Soc. Lond., Spec. Publ. 233, 181–191.

Arts, R., Vandeweijer, V., Hofstee, C., Pluymaekers, M., Loeve, D., Kopp, A., Plug, W., 2012. The feasibility of CO_2 storage in the depleted P18-4 gas field offshore the Netherlands (the ROAD project). Int. J. Greenhouse Gas Control 11, S10–S20.

Barton, N., 1973. Review of a new shear-strength criterion for rock joints. Eng. Geol. 7, 287–332.

Baudon, C., Cartwright, J., 2008. The kinematics of reactivation of normal faults using high resolution throw mapping. J. Struct. Geol. 30, 1072–1084.

Bentham, M., Green, A., Gammer, D., 2013. The occurrence of faults in the Bunter Sandstone Formation of the UK sector of the Southern North Sea and the potential impact on storage capacity. Energy Procedia 37, 5101–5109.

Bertoni, C., Cartwright, J.A., 2005. 3D seismic analysis of circular evaporite dissolution structures, Eastern Mediterranean. J. Geol. Soc. 162, 909–926.

Blenkinsop, T.G., 2004. Orebody geometry in lode gold deposits from Zimbabwe: implications for fluid flow, deformation and mineralization. J. Struct. Geol. 26, 1293–1301.

Bouw, L., Essink, G., 2003. Fluid flow in the northern Broad Fourteens Basin during Late Cretaceous inversion. Neth. J. Geosci. (Geol. Mijnb.) 82, 55–69.

Brown, A.R., Brown, A.R., Brown, A.R., Brown, A.R., 2004. Interpretation of three-dimensional seismic data. American Association of Petroleum Geologists, Tulsa.

Cartwright, J., Huuse, M., Aplin, A., 2007. Seal bypass systems. AAPG Bull. 91, 1141–1166.

Cartwright, J., Santamarina, C., 2015. Seismic characteristics of fluid escape pipes in sedimentary basins: implications for pipe genesis. Mar. Pet. Geol. 65, 126–140.

Cartwright, J., Stewart, S., Clark, J., 2001. Salt dissolution and salt-related deformation of the Forth Approaches Basin, UK North Sea. Mar. Pet. Geol. 18, 757–778.

Cartwright, J.A., Trudgill, B.D., Mansfield, C.S., 1995. Fault growth by segment linkage: an explanation for scatter in maximum displacement and trace length data from the Canyonlands Grabens of SE Utah. J. Struct. Geol. 17, 1319–1326.

Cathles, L., Su, Z., Chen, D., 2010. The physics of gas chimney and pockmark formation, with implications for assessment of seafloor hazards and gas sequestration. Mar. Pet. Geol. 27, 82–91.

Cawley, S., Saunders, M., Le Gallo, Y., Carpentier, B., Holloway, S., Kirby, G., Bennison, T., Wickens, L., Wickramaratna, R., Bidstrup, T., 2015. The NGCAS project—assessing the potential for EOR and CO_2 storage at the Forties Oilfield, Offshore UK. Carbon Dioxide Capture for Storage in Deep Geologic Formations—Results from the CO Vol. 2, pp. 713–750.

Childs, C., Nicol, A., Walsh, J.J., Watterson, J., 2003. The growth and propagation of synsedimentary faults. J. Struct. Geol. 25, 633–648.

Coward, M., 1995. Structural and tectonic setting of the Permo-Triassic basins of northwest Europe. Geol. Soc. Lond., Spec. Publ. 91, 7–39.

Coward, M., Stewart, S., 1995. Salt-influenced Structures in the Mesozoic–Tertiary Cover of the Southern North Sea, UK.

Curewitz, D., Karson, J.A., 1997. Structural settings of hydrothermal outflow: fracture permeability maintained by fault propagation and interaction. J. Volcanol. Geotherm. Res. 79, 149–168.

De Lugt, I.R., Van Wees, J.D., Wong, T.E., 2003. The tectonic evolution of the southern Dutch North Sea during the Palaeogene: basin inversion in distinct pulses. Tectonophysics 373, 141–159.

Duin, E., Doornenbal, J., Rijkers, R., Verbeek, J., Wong, T.E., 2006. Subsurface structure of the Netherlands—results of recent onshore and offshore mapping. Neth. J. Geosci. 85, 245.

Farmer, I.W., Jumikis, A.R., 1968. Engineering Properties of Rocks. E. & F. N. Spon Limited, 11 New Fetter Lane, London E.C.4.

Ferrill, D.A., Stamatakos, J.A., Sims, D., 1999. Normal fault corrugation: implications for growth and seismicity of active normal faults. J. Struct. Geol. 21, 1027–1038.

Frey-Martinez, J., Cartwright, J., Hall, B., Huuse, M., 2007. Clastic Intrusion at the Base of Deep-Water Sands: A Trap-Forming Mechanism in the Eastern Mediterranean.

Frikken, H.W., 1999. Reservoir-Geological Aspects of Productivity and Connectivity of Gasfields in the Netherlands. Delft University of Technology, TU Delft.

Gay, A., Lopez, M., Berndt, C., Seranne, M., 2007. Geological controls on focused fluid flow associated with seafloor seeps in the Lower Congo Basin. Mar. Geol. 244, 68–92.

Ge, H., Jackson, M.P., 1998. Physical modeling of structures formed by salt withdrawal: implications for deformation caused by salt dissolution. AAPG Bull. 82, 228–250.

Gerling, P., Geluk, M., Kockel, F., Lokhorst, A., Lott, G., Nicholson, R., 1999. 'NW European Gas Atlas'—new implications for the Carboniferous gas plays in the western part of the Southern Permian Basin. Geological Society, London, Petroleum Geology Conference Series. Geological Society of London, pp. 799–808.

Grollimund, B., Zoback, M.D., Wiprut, D.J., Arnesen, L., 2001. Stress orientation, pore pressure and least principal stress in the Norwegian sector of the North Sea. Pet. Geosci. 7, 173–180.

Handin, J., Hager Jr., R.V., Friedman, M., Feather, J.N., 1963. Experimental deformation of sedimentary rocks under confining pressure: pore pressure tests. AAPG Bull. 47, 717–755.

Hardman, R., Booth, J., 1991. The significance of normal faults in the exploration and production of North Sea hydrocarbons. Geol. Soc. Lond., Spec. Publ. 56, 1–13.

Healy, D., Blenkinsop, T.G., Timms, N.E., Meredith, P.G., Mitchell, T.M., Cooke, M.L., 2015. Polymodal faulting: time for a new angle on shear failure. J. Struct. Geol. 80, 57–71.

Heidbach, O., Tingay, M., Barth, A., Reinecker, J., Kurfeß, D., Müller, B., 2008. The World Stress Map Database Release 2008 (2008). http://dx.doi.org/10.1594/GFZ WSM. Rel2008.

Heim, S., Lutz, R., Nelskamp, S., Verweij, H., Kaufmann, D., Reinhardt, L., 2013. Geological evolution of the North Sea: cross-border basin modeling study on the Schillground High. Energy Procedia 40, 222–231.

Herber, R., De Jager, J., 2010. Geoperspective oil and gas in the Netherlands—is there a future? Neth. J. Geosci. 89, 91–107.

Hillis, R., Nelson, E., 2005. In situ stresses in the North Sea and their applications: petroleum geomechanics from exploration to development. Geological Society, London, Petroleum Geology Conference Series. Geological Society of London, pp. 551–564.

Hooper, R.J., Goh, L.S., Dewey, F., 1995. The inversion history of the northeastern margin of the Broad Fourteens Basin. Geol. Soc. Lond., Spec. Publ. 88, 307–317.

Hustoft, S., Bünz, S., Mienert, J., 2010. Three-dimensional seismic analysis of the morphology and spatial distribution of chimneys beneath the Nyegga pockmark field, offshore mid-Norway. Basin Res. 22, 465–480.

Hustoft, S., Mienert, J., Bünz, S., Nouzé, H., 2007. High-resolution 3D-seismic data indicate focussed fluid migration pathways above polygonal fault systems of the mid-Norwegian margin. Mar. Geol. 245, 89–106.

Jackson, C.A.-L., Rotevatn, A., 2013. 3D seismic analysis of the structure and evolution of a salt-influenced normal fault zone: a test of competing fault growth models. J. Struct. Geol. 54, 215–234.

Kattenhorn, S.A., Pollard, D.D., 2001. Integrating 3-D seismic data, field analogs, and mechanical models in the analysis of segmented normal faults in the Wytch Farm oil field, southern England, United Kingdom. AAPG Bull. 85, 1183–1210.

Kopf, A.J., 2002. Significance of mud volcanism. Rev. Geophys. 40 2-1–2-52.

Leveille, G.P., Knipe, R., More, C., Ellis, D., Dudley, G., Jones, G., Fisher, Q.J., Allinson, G., 1997. Compartmentalization of Rotliegendes gas reservoirs by sealing faults, Jupiter Fields area, southern North Sea. Geol. Soc. Lond., Spec. Publ. 123, 87–104.

Lokhorst, A., Wildenborg, T., 2005. Introduction on CO_2 geological storage—classification of storage options. Oil Gas Sci. Technol. 60, 513–515.

Løseth, H., Gading, M., Wensaas, L., 2009. Hydrocarbon leakage interpreted on seismic data. Mar. Pet. Geol. 26, 1304–1319.

Maione, S.J., Pickford, S., 2001. Discovery of ring faults associated with salt withdrawal basins, Early Cretaceous age, in the East Texas Basin. The Leading Edge, pp. 818–829.

Mansfield, C., Cartwright, J., 1996. High resolution fault displacement mapping from three-dimensional seismic data: evidence for dip linkage during fault growth. J. Struct. Geol. 18, 249–263.

McFarland, J.M., Morris, A.P., Ferrill, D.A., 2012. Stress inversion using slip tendency. Comput. Geosci. 41, 40–46.

Morris, A., Ferrill, D.A., Henderson, D.B., 1996. Slip-tendency analysis and fault reactivation. Geology 24, 275–278.

Nalpas, T., Le Douaran, S., Brun, J.-P., Unternehr, P., Richert, J.-P., 1995. Inversion of the Broad Fourteens Basin (offshore Netherlands), a small-scale model investigation. Sediment. Geol. 95, 237–250.

Neele, F., ten Veen, J., Wilschut, F., Hofstee, C., 2012. Independent assessment of high-capacity offshore CO_2 storage options. TNO-Report, RCI-ISA Phase 3.

Newnes, S., 2014. Tectonic Reactivation as a Control on Gas and CO_2 Leakage in the Rotliegend Reservoir, Dutch North Sea. Cardiff University, Unpublished master's thesis.

Omosanya, K.D.O., Alves, T.M., 2014. Mass-transport deposits controlling fault propagation, reactivation and structural decoupling on continental margins (Espírito Santo Basin, SE Brazil). Tectonophysics 628, 158–171.

Osborne, M.J., Swarbrick, R.E., 1997. Mechanisms for generating overpressure in sedimentary basins: a reevaluation. AAPG Bull. 81, 1023–1041.

Oudmayer, B.C., De Jager, J., 1993. Fault reactivation and oblique-slip in the Southern North Sea. In: Parker, J.R. (Ed.), Petroleum Geology of Northwest Europe: Proceedings of the 4th Conference. The Geological Society, London, pp. 1281–1290.

Passey, Q., Creaney, S., Kulla, J., Moretti, F., Stroud, J., 1990. A practical model for organic richness from porosity and resistivity logs. AAPG Bull. 74, 1777–1794.

Penge, J., Taylor, B., Huckerby, J., Munns, J., 1993. Extension and salt tectonics in the East Central Graben. Geological Society, London, Petroleum Geology Conference Series. Geological Society of London, pp. 1197–1209.

Price, N.J., Cosgrove, J.W., 1990. Analysis of Geological Structures. Cambridge University Press, Cambridge.

Stewart, S.A., 1999. Seismic interpretation of circular geological structures. Pet. Geosci. 5, 273–285.

Stewart, S.A., 2006. Implications of passive salt diapir kinematics for reservoir segmentation by radial and concentric faults. Mar. Pet. Geol. 23, 843–853.

Stewart, S.A., Coward, M.P., 1995. Synthesis of salt tectonics in the southern North Sea, UK. Mar. Pet. Geol. 12, 457–475.

Underhill, J.R., 2004. Earth science: an alternative origin for the 'Silverpit crater'. Nature 428.

Underhill, J.R., 2009. Role of intrusion-induced salt mobility in controlling the formation of the enigmatic 'Silverpit Crater', UK Southern North Sea. Pet. Geosci. 15, 197–216.

Van Adrichem Boogaert, H., Kouwe, W., 1993. Stratigraphic nomenclature of the Netherlands, revision and update by RGD and NOGEPA. Med. Rijks Geol. Dienst. 50, 1–40.

Van Adrichem Boogaert, H.A., Kouwe, W.F.P., 1994-1997. Stratigraphic nomenclature of the Netherlands, revision and update by RGD and NOGEPA. Mededelingen Rijks Geologische Dienst, Section A-J.

van Gent, H.W., Back, S., Urai, J.L., Kukla, P.A., Reicherter, K., 2009. Paleostresses of the Groningen area, the Netherlands—results of a seismic based structural reconstruction. Tectonophysics 470, 147–161.

Van Hulten, F.F.N., 2010a. Can stratigraphic plays change the petroleum exploration outlook of the Netherlands? Geological Society, London, Petroleum Geology Conference Series. Geological Society of London, pp. 261–275

Van Hulten, F.F.N., 2010b. Geological factors effecting compartmentalization of Rotliegend gas fields in the Netherlands. Geol. Soc. Lond., Spec. Publ. 347, 301–315.

Van Rensbergen, P., Rabaute, A., Colpaert, A., Ghislain, T.S., Mathijs, M., Bruggeman, A., 2007. Fluid migration and fluid seepage in the Connemara Field, Porcupine Basin interpreted from industrial 3D seismic and well data combined with high-resolution site survey data. Int. J. Earth Sci. 96, 185–197.

Van Wees, J.-D., Stephenson, R., Ziegler, P., Bayer, U., McCann, T., Dadlez, R., Gaupp, R., Narkiewicz, M., Bitzer, F., Scheck, M., 2000. On the origin of the southern Permian Basin, central Europe. Mar. Pet. Geol. 17, 43–59.

Van Wijhe, D.V., 1987. Structural evolution of inverted basins in the Dutch offshore. Tectonophysics 137, 171–219.
Verweij, J.M., Simmelink, H.J., 2002. Geodynamic and hydrodynamic evolution of the Broad Fourteens Basin (The Netherlands) in relation to its petroleum systems. Mar. Pet. Geol. 19, 339–359.
Verweij, J.M., Simmelink, H.J., Van Balen, R.T., David, P., 2003. History of petroleum systems in the southern part of the Broad Fourteens Basin. Neth. J. Geosci. 82, 71–90.
Weijermars, R., 2013. Economic appraisal of shale gas plays in Continental Europe. Appl. Energy 106, 100–115.
Wiprut, D., Zoback, M.D., 2000. Fault reactivation and fluid flow along a previously dormant normal fault in the northern North Sea. Geology 28, 595–598.
Wiprut, D., Zoback, M.D., 2002. Fault reactivation, leakage potential, and hydrocarbon column heights in the northern North Sea. Norwegian Petroleum Society Special Publications Vol. 11, pp. 203–219.
Wong, T.E., Parker, N., Horst, P., 2001. Tertiary sedimentary development of the Broad Fourteens area, the Netherlands. Geol. Mijnb. 80, 85–94.
Ziegler, P., 1992. North Sea rift system. Tectonophysics 208, 55–75.
Ziegler, P.A., 1990. Geological atlas of western and central Europe. Shell Internationale Petroleum, second ed. Maatschappij B.V., The Hague.
Zoback, M.D., 2010. Reservoir Geomechanics. Cambridge University Press.